Development of microfluidic passive flow assays for point-of-care quantification of chronic kidney disease biomarkers in urine and serum

By

Dumitru Tomsa

A Thesis submitted to the Faculty of Graduate Studies of

The University of Manitoba

in partial fulfillment of the requirements of the degree of

MASTER OF SCIENCE

Biomedical Engineering Program

University of Manitoba

Winnipeg

List of publications

A significant part of this thesis (i.e., Chapter 2 and Chapter 3) is based on the following peer-reviewed journal and conference publications while the publication [1] is only providing background for the current work.

Journal Articles

1. Wu, J., **Tomsa, D.**, Zhang, M., Komenda, P., Tangri, N., Rigatto, C., & Lin, F. (2018). "*A passive mixing microfluidic urinary albumin chip for chronic kidney disease assessment".* **ACS Sensors**, 3(10), 2191–2197.
2. **Tomsa, D.**, Liu, Y., Stefanson, A., Lin, F. et al. "*A passive flow microreactor for urine creatinine test".* **Microsyst Nanoeng** 11, 56 (2025).
3. **Tomsa, D.**, Liu, Y., Abolfathi, A.H., Lin, F. et al. "*Integrated microfluidic immunoassays for point-of-care diagnostic measurement of human serum Cystatin C in chronic kidney disease".* (**Submitted for journal publication. Under review.**)

Conference Proceeding

4. **Tomsa, D.**, Liu, Y., Stefanson, A., Ren, X., Sokoro, A., Komenda, P., Tangri, N., Zahedi, R., Rigatto, C., & Lin, F. **"***A passive flow microreactor for urine creatinine test".* **The 28th International Conference on Miniaturized Systems for Chemistry and Life Sciences (MicroTAS)**, Montreal, Canada, 13-17, October, **2024**

Patent Applications

5. Lin, F., **Tomsa, D.**, Stefanson, A., Ren, X., Liu, Y., Rigatto, C., Komenda, P., Tangri, N. *"Microfluidic urine albumin/creatinine chip (uACR-Chip) for chronic kidney disease evaluation"*, Worldwide Patent application (national phase): WO2023201418A1.

6. Lin, F., Ren, X., **Tomsa, D.**, Stefanson, A., Liu, Y., Rigatto, C., Komenda, P., Tangri, N. *"Paper-based microfluidic chip for measurement of cystatin-C in plasma and serum"*, Worldwide Patent application (national phase): WO202023178416A1.

Abstract

Chronic kidney disease (CKD) significantly affects people's health and life quality and presents a high economic burden worldwide. However, the existing diagnostic test methods remain complicated and cost-prohibitive.

This research addresses critical gaps in CKD diagnostics through the development of innovative microfluidic platforms for point-of-care (PoC) testing. We present complementary approaches targeting key CKD biomarkers: a passive flow microreactor for urinary creatinine measurement (uCR-Chip) and microfluidic devices for serum cystatin C (CYS-C) quantification.

The uCR-Chip employs a 2-phase pressure compensation technique, optimized observation window (OW), and channel network design to control fluidic mixing and chemical reactions precisely. A stable signal is achieved within 7 minutes, with the dynamic range up to 40 mM and a lower limit of detection of 0.521 mM. This performance meets clinical precision requirements and demonstrates acceptable recovery rates in artificial urine matrices, particularly at lower creatinine concentrations, making it highly amenable to integration with previously developed microfluidic urine albumin assays.

For CYS-C, recommended as a superior estimated glomerular filtration rate (eGFR) biomarker due to minimal influence from non-filtration factors like muscle mass, we developed a PDMS-based immunoturbidity chip enabling side-scattering optical measurement. We demonstrated that the CYS-C chip meets the clinical requirements for detection range and limits while integrated into a custom-developed reader for PoC applications. Validation studies using CKD patient samples demonstrated comparable

agreement levels with the traditional well plate-based immunoturbidity assay test results, determining eGFR range across clinically relevant group criteria.

Together, these microfluidic platforms offer viable solutions for decentralized CKD assessment, providing potential technology for measuring various disease biomarkers with advantages in accessibility, speed, and precision compared to existing clinical methods.

Acknowledgments

First and foremost, I would like to express my deepest gratitude to my supervisor, Professor Francis Lin, for his unwavering support, expert guidance, and constructive feedback throughout every stage of this research. I am also grateful to my thesis committee—Dr. Elham Salimi and Dr. Claudio Rigatto—for their insightful comments and suggestions, which have greatly strengthened this work.

I would like to thank the members of Dr. Lin's Lab, especially Dr. Yang Liu, Dr. Amanda Stefanson, Dr. Xiaoou Ren, Dr. Jiandong Wu, Amir Hossein Abolfathi, and Nicholas Palmerley, for their collaboration, technical assistance, and many stimulating discussions. Special thanks go to Dr. Peiqing Wang, Maiko Langelaar, Aymsley Bishop-Mahon, Susan Beshta, and Milijana Prstojevic at the Facility of Physics for help with technical and administrative work.

I also would like to thank the Nano-Systems Fabrication Laboratory at the University of Manitoba for their support and Dwayne Chrusch for his patience and enthusiasm teaching me the use of the photolithography equipment. I thank AbdulRazaq A. H. Sokoro, Paul Komenda, and Navdeep Tangri for clinical advice.

This project was made possible by financial support from My Health Logic, Inc. (a subsidiary of Marizyme, Inc.) and AssureCKD, Inc. through sponsored research agreements. I thank the Natural Sciences and Engineering Research Council of Canada (NSERC) and Graduate Enhancement of Tri-Agency Stipends (GETS) program for partial stipend support. I also acknowledge the resources provided by the Manitoba Centre for Proteomics and Systems Biology.

On a personal note, I am deeply indebted to my parents—Lilia and Iulian Tomsa—for their patience, encouragement, and love throughout this journey.

Table of Contents

List of Tables and Figures

List of Abbreviations

2-PPC	2-phase pressure compensation
3D	3 Dimension
CDC	Centers for Disease Control and Prevention
CKD	Chronic Kidney Disease
CKM syndrome	Cardiovascular-Kidney-Metabolic syndrome
CYS-C	Cystatin C
DI H_2O	Deionized water
eGFR	Estimated Glomerular Filtration Rate
eGFRcys-c	Cystatin C concentration-based Estimated Glomerular Filtration Rate
eGFRcr	Creatinine concentration-based Estimated Glomerular Filtration Rate
ELISA	Enzyme-Linked Immunosorbent Assay
FWHM	Full Width Half Maximum
GFR	Glomerular Filtration Rate
LED	Light Emitting Diode
LOD	Limit of Detection
OW	Observation Window
PDMS	Polydimethylsiloxane

PENIA	Particle-Enhanced Nephelometric Immunoassay
PETIA	Particle-Enhanced Turbidimetric Immunoassay
PoC	Point of Care
R1	Reagent 1
R2	Reagent 2
uACR	Urinary Albumin to Creatinine Ratio
uAL-Chip	Urinary Albumin Chip
uCR-Chip	Urinary Creatinine Chip
WHO	World Health Organization

Chapter 1: Introduction

1.1 Overview of Chronic Kidney Disease

Chronic kidney disease (CKD) is an extremely common condition that affects approximately 10% of the world population. It is projected that CKD will become a top 5 cause of death by the year 2040 at current increasing death rates associated with that condition[1].

Along with many other functions, kidneys play a crucial role in the removal of waste products from blood. Hundreds of thousands of filtration units called glomeruli are filtering ~125 mL of blood each minute. In this process, cells and large protein molecules are separated from small ions, water, and waste molecules. Any useful constituents are reabsorbed back in the bloodstream, and the rest becomes urine. Consequently, the concentrations of some of the waste molecules and proteins in blood and urine samples are used to estimate the efficiency of the glomerular filtration rate (eGFR). The kidney filtration rate reduction for an extensive period of time over 3 months is an indicator of CKD. The diagnostics typically involve evaluation of urine and serum samples.

In urine samples, the most common biomarkers are albumin and creatinine. Albumin is one of the most common proteins in human blood. Being a large protein molecule, albumin is filtered by healthy kidneys; therefore, its presence in a urine sample is an indicator of kidney damage. Since production of urine varies over time and depends on metabolic processes in the human body, there has to be a correction factor used for the albumin concentration. The standard biomarker used for that purpose is creatinine, a waste product of digestion and metabolism that is released at a constant rate. In standard clinical practice,

the ratio between albumin and creatinine (uACR) is used to estimate the level of kidney damage.

In blood samples, creatinine concentration is the most common measure of kidney function in clinical practice. High concentrations of creatinine can be a signal that kidneys are not filtering the waste products at the proper rate. Despite it being a common biomarker, creatinine concentration is affected by several factors like sex, age, and muscle mass. That often complicates the diagnostics process. After many years of research, a novel biomarker called cystatin C (CYS-C) has been approved that is more accurate and more specific to CKD. CYS-C is a small protein molecule produced at a constant rate by all nucleated cells of the body. It is also not affected by sex, age, or muscle mass. The most recent CKD diagnostic protocols recommend using a formula that uses both serum creatinine and CYS-C (CKD-EPI Creatinine-Cystatin Equation (2021)), as it was shown to provide an even more accurate GFR estimate.

1.2 Overview of Point of Care Testing in CKD

The most common types of assays for laboratory use are ELISA (enzyme-linked immunosorbent assay), which provides accurate and quantitative measures. ELISA kits are available for many different biomarkers, including creatinine and CYS-C, but the main disadvantages are: 1. High cost. A single assay kit designed for one 96-well plate can cost $700 or more. 2. Complexity of operation. One ELISA kit often contains multiple reagents that must be stored at -20°C and need to be handled with extreme care by trained personnel. These properties of ELISA assay kits make them not suitable for point-of-care diagnostics despite the high sensitivity. Alternative colorimetric detection methods for creatinine are the assay kits that are using the Jaffe reaction, for example, Randox 510. It is a well-known

reaction between picric acid and creatinine that is changing its color from yellow to orange. The advantage is that it requires only two reagent solutions that can be stored at 4°C or room temperature, and the time of reaction is between 5 and 10 minutes. For CYS-C measurement, turbidimetric immunoassays can be used that contain microparticles coated with specific antibodies that attract the target protein and expand in size. Similarly, this type of assay consists of 2 reagents and can be stored at 4°C.

The list of criteria for PoC testing was introduced by the World Health Organization and has an acronym REASSURED (Real-time connectivity, Ease of specimen collection, Affordable, Sensitive, Specific, User-friendly, Rapid and robust, Equipment-free and Deliverable to end-users). Current methods used for CKD biomarker detection satisfy only a few of the listed criteria. Among commercially available diagnostic tools, DCA Vantage from Siemens and Afinion ACR from Abbott are trying to bring testing closer to the point of care. Yet they still do not qualify as true PoC tools because of the high cost, bulky equipment, and requirement for trained personnel to operate. Other methods like dipstick tests from Siemens Clinitek or the "Minuteful kidney test" can only provide qualitative or semi-quantitative results, and despite their simplicity and low cost, they cannot be used to make serious diagnostic decisions. In addition, the Siemens Clinitek also requires a large tabletop reader, which limits its PoC use.

1.3 Overview of Microfluidics Development in CKD Diagnosis

The researchers around the world continue the work on developing other methods of detection for creatinine and CYS-C. Though most of these methods currently exist only in the lab settings. One common approach that researchers are using is electrochemical detection. The general idea is the design of a molecule-specific electrode that, with the help

of cyclic voltammetry, can estimate the concentration of a target molecule in a sample. There is a large number of techniques and materials that are used in the designs of such electrodes. Among them are electrodes covered with molecularly imprinted polymers (MIPs)[2,3], electrodes coated with nanoparticles that can immobilize CYS-C antibodies[4], and composite sensing film that works by measuring the reaction of creatinine with an enzyme[5].

Other methods use lateral flow immunoassays (LFIA) to detect biomarkers such as creatinine or CYS-C. Often LFIAs are using specific antibodies conjugated with gold nanoparticles for colorimetric detection[6]. Others use fluorescent dyes or even develop and synthesize new molecules for biomarker detection[7]. Each of these approaches has its own advantages and disadvantages and often requires further investigation and optimization.

1.4 Motivation

The current procedure of CKD diagnostics presents significant challenges that motivate the development of more accessible diagnostic solutions. The standard procedure of diagnostics requires multiple visits and consists of the following steps: 1) Visit to the doctor's office to discuss the patient's health concerns, 2) Urine/blood sample collection in the lab, usually in a different location, 3) Approximately one week delay until the samples are analyzed and the results are sent to the doctor, 4) Follow-up visit to the doctor's office to discuss the sample testing results and prescribe treatment. Such a diagnostic process greatly complicates the patient experience, especially in resource-poor rural areas where patients travel long distances to access labs and care. Most labs use large and expensive analyzers like the Siemens BN II System, Roche Cobas Mira Plus Chemistry Analyzer, Tina-quant Cystatin C Gen. 2, AU480 Chemistry Analyzer. These machines can perform up to 1000s of sample analyses per hour. To make the usage of such equipment economically viable, it must

be a part of a centralized system with developed logistics to regularly collect and deliver samples from thousands of patients every day. Unfortunately, no matter how well such logistics are fine-tuned, they are not able to satisfy the need for PoC sample analysis that is required for CKD patients.

These challenges directly motivate our research into portable PoC diagnostic solutions. By developing a small, low-cost, and user-friendly microfluidic platform, we aim to enable immediate sample analysis at the patient's location and eliminate delays between testing and treatment decisions. We believe that our passive microfluidic solution addresses the critical need for accessible diagnostics and can extend quality CKD care to underserved populations. Our research specifically targets the development of a passive microfluidic chip that can detect creatinine and CYS-C, the key CKD biomarkers, with comparable accuracy to laboratory equipment but at a fraction of the size and cost.

1.5 Research Objectives

The objective of this work is to investigate ideas and techniques that have the potential to bring the CKD diagnostic tools to the patients. The objective of this thesis is to investigate microfluidic approaches for PoC diagnostics of CKD. To this end, the work is organized into two manuscripts. Chapter 2 presents the design and fabrication of a low-cost, passive-flow microreactor for creatinine measurement with optimized observation (OW) and channel geometry for controlled mixing ratio and reaction time. The analytical characterization presents the data on the theoretical and practical performance of the microreactor, its stability, dynamic range, and limit of detection (LOD). The chip performance is evaluated and compared to commercial measuring systems using artificial urine and real clinical samples.

Chapter 3 presents the microfluidic chip design for an immunoturbidimetric cystatin C assay and its protocol optimization. The nephelometric readout is described in terms of the general principle of operation as well as detailed design considerations. The overall performance is evaluated using CYS-C in simple buffer and clinical blood samples with a traditional 96-well plate test as a reference.

Collectively, the goal of these studies is to evaluate passive and immunoassay-based microfluidic strategies, assess the compromises among ease of use, economic feasibility, and assay performance, and define guiding principles for designing the next generation of PoC platforms.

1.6 References

1. Kövesdy, C. P. (2022). *Epidemiology of chronic kidney disease: an update 2022*. **Kidney International Supplements**, 12(1), 7–11.
2. Stojanovi´c, Z., Erdössy, J., Keltai, K., Scheller, F. W., and Gyurcs´anyi, R. E. *"Electrosynthesized molecularly imprinted polyscopoletin nanofilms for human serum albumin detection,"* **Analytica Chimica Acta**, vol. 977, pp. 1–9, Jul. 2017.
3. Gomes, R. S., Gomez-Rodr´ıguez, B. A., Fernandes, R., Sales, M. G. F., Moreira, F. T. C., and Dutra, R. F. *"Plastic antibody of Polypyrrole/Multiwall carbon nanotubes on Screen-Printed electrodes for cystatin C detection,"* **Biosensors**, vol. 11, no. 6, p. 175, May 2021.
4. Chakraborty, T., Das, M., Lin, C. Y., and Kao, C., *"Electrochemical detection of cystatin C by oriented antibody immobilization on streptococcal protein G–modified ZIF-8-Cu1xNix(OH)2@Cu core-shell nanostructured electrode,"* **Materials Today Chemistry**, vol. 27, p. 101273, Jan. 2023.
5. Do, J.-S., and Chang, Y.-C., *"Optimizing the sensing performance of amperometric creatinine detection based on creatinine deiminase/Nafion®-nanostructured polyaniline composite film by mixture design method,"* **Sensors and Actuators Reports**, vol. 5, p. 100135, Jun. 2023.
6. Chotithammakul, S., Cortie, M. B., and Pissuwan, D., *"Comparison of Single- and Mixed-Sized gold nanoparticles on lateral flow assay for albumin detection,"* **Biosensors**, vol. 11, no. 7, p. 209, Jun. 2021.

7. Azeman, N. H., et al., *"Synthesis of a 1,4-Bis[2-(5-thiophen-2-yl)-1-benzothiophene]-2,5-dioctyloxybenzene pentamer for creatinine detection,"* **Asian Journal of Organic Chemistry**, vol. 10, no. 9, pp. 2406–2417, Aug. 2021.

Chapter 2: A passive flow microreactor for urine creatinine test

This chapter is based on the following publication:

Tomsa, D., Liu, Y., Stefanson, A. *et al. "A passive flow microreactor for urine creatinine test".* **Microsyst Nanoeng** 11, 56 (2025).

In this project, we developed a passive flow microreactor for colorimetric urine creatinine measurement (uCR-Chip), which is highly amenable to integration with our previously developed microfluidic urine albumin assay. The color signal was measured by a simple USB microscope-based platform to quantify creatinine concentration in the sample. The developed assay achieved a dynamic linear detection range up to 40 mM and a lower LOD of 0.521 mM, meeting clinical requirements (comparable to existing PoC systems). The microreactor was validated using creatinine standards spiked into commercial artificial urine that mimics a physiological matrix. Our results showed an acceptable recovery rate and low matrix effect, especially for the low creatinine concentration range in comparison to a commercial

In this study, I assembled the system, conducted the experiments, analyzed the data, and wrote the manuscript.

2.1 Abstract

CKD significantly affects people's health and quality of life and presents a high economic burden worldwide. There are well-established biomarkers for CKD diagnosis. However, the existing routine tests for CKD are lab-based and governed by strict regulations. Creatinine is commonly measured as a filtration biomarker in blood to determine estimated eGFR, as well as a normalization factor to calculate urinary Albumin-to-Creatinine Ratio (uACR) for CKD evaluation. In this study, we developed a passive flow microreactor for colorimetric urine creatinine measurement (uCR-Chip), which is highly amenable to integration with our previously developed microfluidic urine albumin assay. The combination of the 2-phase pressure compensation (2-PPC) technique and microfluidic channel network design accurately controls the fluidic mixing ratio and chemical reaction. Together with an optimized OW design, a uniform and stable detection signal was achieved within 7 minutes. The color signal was measured by a simple USB microscope-based platform to quantify creatinine concentration in the sample. The combination of the custom in-house photomask production techniques and dry-film photoresist-based lithography enabled rapid iterative design optimization and precise chip fabrication. The developed assay achieved a dynamic linear detection range up to 40 mM and a lower LOD of 0.521 mM, meeting the clinical precision requirements (comparable to existing PoC systems). The microreactor was validated using creatinine standards spiked into commercial artificial urine that mimics a physiological matrix. Our results showed an acceptable recovery rate and low matrix effect, especially for the low creatinine concentration range in comparison to a commercial PoC uACR test. Altogether, the developed uCR-Chip offers a viable PoC test

for CKD assessment and provides a potential platform technology to measure various disease biomarkers.

2.2 Introduction

CKD is characterized by kidney damage or loss of function that persists for at least 3 months[1]. Kidney function declines over time, causing fluid, electrolyte, and waste buildup in the body. CKD affects over 800 million individuals around the world or 8-16% of the global population, making it a major cause of death, particularly in lower- and middle-income nations[2–5]. CKD is closely associated with heart disease, high blood pressure, diabetes, and cardiovascular-kidney-metabolic (CKM) syndrome[6,7] as well as adverse outcomes in hospitalized patients[8]. Untreated CKD can progress to kidney failure, necessitating burdensome and expensive treatments like peritoneal dialysis, hemodialysis, or kidney transplantation, placing a heavy burden on patients and health systems[2]. CKD can be treated effectively, and the consequences are preventable if diagnosed at an early stage[9]. However, fewer than 5% of those in the early stages of CKD are aware of their disease[10]. Effective screening strategies with at-risk patients could increase the CKD identification and are predicted to be cost-effective. The two key diagnostic markers for CKD are the eGFR and the uACR, both involving measuring creatinine as a biomarker. CKD is diagnosed based on eGFR, 60 mL/min/1.73 m^2 persisting for >3 months, or the presence of albuminuria (ACR > 3 mg/g) persistent for at least 3 months or more[11]. In addition, uACR is an important measurement for identifying kidney damage in patients with kidney-related diseases. The urine tests are often the first step in CKD diagnosis and a critical part of follow-up management[12]. As a non-invasive assay, urine tests not only provide diagnostic and staging data for CKD, but also generate insights into prognostics and progression of the disease[13].

Furthermore, low levels of creatinine in urine can indicate low muscle mass and thus are considered a prognostic factor for predicting cardiovascular disease and CKD outcomes[14].

Creatinine is a small molecule (0.113 kDa) by-product of creatine metabolism in muscle tissue. Muscle creatine is used to produce energy in the form of ATP via the enzymatic conversion to phosphocreatine. Creatinine is formed by spontaneous, non-enzymatic degradation of creatine, which is then released into the bloodstream and ultimately filtered by the kidneys as a urinary waste product[15]. As creatinine is secreted at a relatively constant rate compared to urine albumin and is commonly used as a normalization factor in urinary analysis, the urine ACR is a more accurate CKD screening and diagnostic marker than urine albumin alone[11].

Clinical urine tests are typically conducted in centralized labs, requiring patients to pay a separate lab visit, and the sample-to-result time is long[16]. A rapid, cost-effective, easy-to-use, and accurate PoC urine test is highly desirable[17]. Dipstick strips a commonly used PoC urine test tools, which provide qualitative or semi-quantitative test results[17]. More accurate PoC urine tests are available; however, the current systems remain cost prohibitive and require specialized skills[18]. The powerful potential of microfluidic devices for PoC diagnostic applications lies in the miniaturization of chemical assays and the simplification of their use, which is the cornerstone of their demonstrated promise to fully address the well-accepted ASSURED criteria for PoC diagnostics[19]. Toward this direction, we previously developed a passive microfluidic device for quantitative urine albumin measurement at very low cost (uAL-Chip) and validated its effective use for testing clinical CKD samples[20]. Because of the importance of urine creatinine to determine uACR, a passive microfluidic device similar to the uAL-Chip for urine creatinine measurement is highly desirable.

Therefore, in the current study, we further developed a passive flow microreactor for measuring urine creatinine (uCR-Chip) based on the Jaffe reaction[21,22]. The uCR-Chip integrates the oil coverage-based 2-phase pressure compensation (2-PPC) technique with optimized microfluidic channel designs to enable highly controlled fluidic mixing and chemical reaction, leading to rapid stabilization of the colorimetric detection signal. Here, we present the details of the uCR-Chip design, fabrication, optimization, and test methodology, as well as its technical characterization and validation results.

2.3 Results

2.3.1 Controlled passive flow mixing and chemical reaction

The Jaffe reaction between creatinine and picric acid in an alkaline medium produces the Janovsky complex, which exhibits a distinct orange color by absorbing light in the wavelength range of 490 nm to 510 nm[22]. The low reagent cost and simplicity of this reaction make it an attractive colorimetric method for quantifying creatinine concentration in urine and blood. Therefore, the main requirements for the Jaffe microreactor are to completely mix the sample with the reagents at a defined ratio, control the reaction time, and allow for simple and reliable colorimetric signal readout, which guided the design, fabrication, and operation of the uCR-Chip.

Theoretically, the hydraulic resistance of the microfluidic channel is directly proportional to the channel length (**Eq. 1** for microfluidic channels with rectangular cross section[23,24]).

$$R = \frac{12\mu L}{wh^3}\left[1 - \frac{h}{w}\left(\frac{192}{\pi^5}\sum_{n=1,3,5}^{\infty}\frac{1}{n^5}\tanh\left(\frac{n\pi w}{2h}\right)\right)\right]^{-1} \quad \textbf{Eq. 1}$$

where R is the hydraulic resistance, L is the channel length, w is the channel width, h is the channel height, and μ is the viscosity of the fluid.

Therefore, the volumetric flow rate is inversely proportional to the channel resistance.

$$Q = \frac{P_2 - P_1}{R} \qquad \textbf{Eq. 2}$$

Where Q is the flow rate; *P2-P1* is the pressure difference between the two ends of the channel.

Consequently, the mixing ratio between the sample and reagent can be determined by designing the inlet channels with the inverted length ratio[20], which guides the inlet channels design.

The uCR-Chip design (**Fig. 2.1a**) includes two inlet wells (one for the Jaffe assay reagent and the other for the sample, respectively); inlet channels with their length designed to match the desired 1:5 sample-to-reagent mixing ratio (i.e. 5L for the sample inlet channel and L for the reagent inlet channel) merging at the T-shaped mixing junction; a mixing channel to allow complete passive flow mixing, directly followed by the reaction channel for the Jaffe reaction over a defined period of time under the specific flow rate; a lenticular

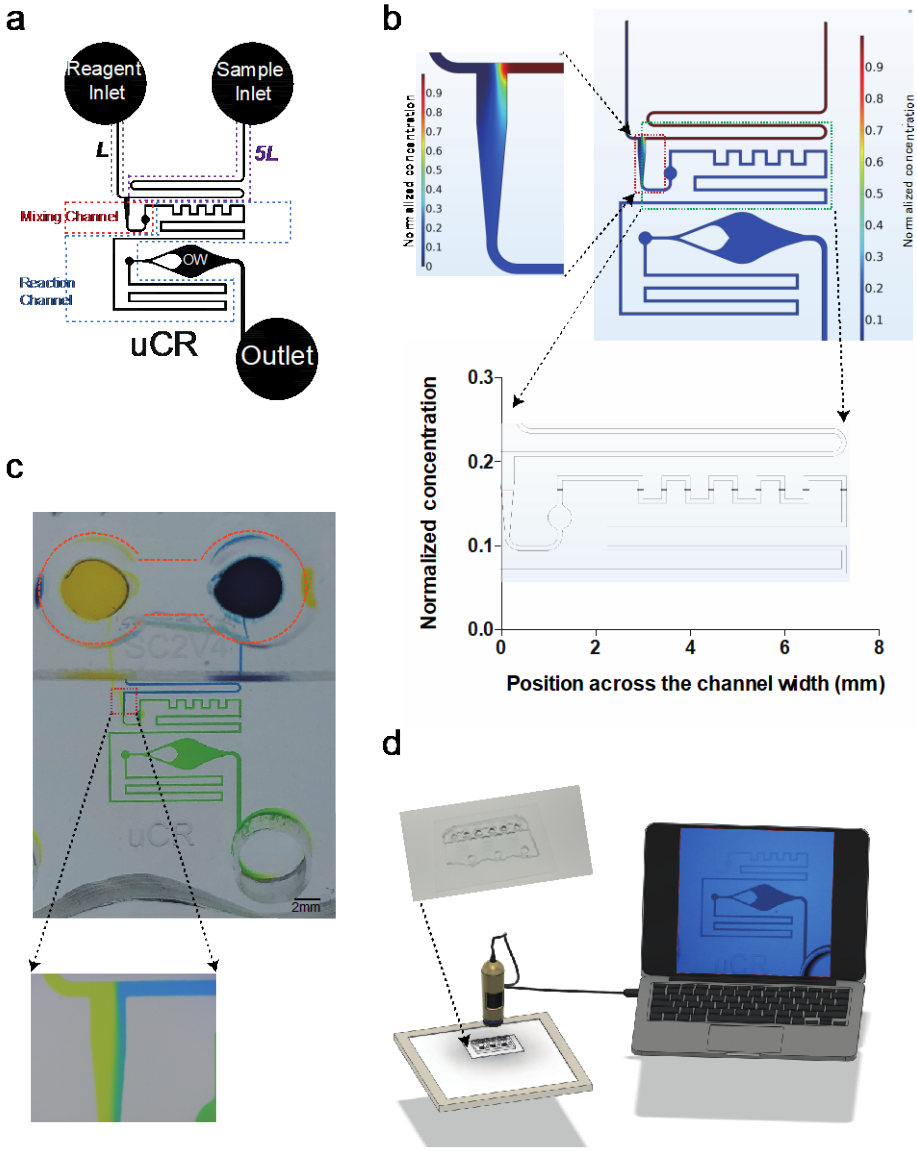

Figure 2.1 Illustration of the uCR-Chip and the test system

a. Schematic illustration of the uCR-Chip showing the reagent inlet, sample inlet, OW, and outlet. The notation L and 5L indicate the channel length from the reagent inlet and the sample inlet channel, respectively, with a ratio of 1:5. The mixing channel originates from the intersection of the two flows, followed by the reaction channel before reaching the OW. **b.** The COMSOL Multiphysics simulation of the flow mixing on the uCR-Chip. Rapid mixing is shown by the color gradient in the mixing channel followed by the uniform color of the diluted concentration in the remaining reaction channel. Controlled mixing at a 1:5 ratio is illustrated in the zoom-in figure. **c.** Experimental testing of the mixing on the uCR-Chip using food color dyes. The rapid mixing is shown by the quick transition to the green color. Controlled mixing at the 1:5 ratio is illustrated in the zoom-in figure. **d.** Illustration of a USB microscope-based colorimetric signal reading system.

shape OW with a flow diverter for colorimetric signal detection and a waste outlet well.

COMSOL Multiphysics was applied to model fluidic mixing under a constant hydrostatic pressure difference between the inlets and outlet in the uCR-Chip (**Fig. 2.1b**). The simulation results verified the expected 1:5 sample-to-reagent mixing ratio, as visualized by the ratiometric division of the mixing channel width into the dark blue and red color flows at the junction (**zoom-in image of the upper panel, Fig. 2.1b**). Complete mixing is demonstrated by the homogeneous blue color toward the end of the mixing channel, which remained stable over the subsequent reaction channel, the OW, and the post-OW channel to the outlet, as shown by both color visualization (**upper panel, Fig. 2.1b**) and the quantitative concentration plot (**bottom panel, Fig. 2.1b**). The normalized final concentration of 0.167 upon complete mixing, as predicted by the simulation, consistently confirmed the 1:5 sample-to-reagent mixing ratio (**bottom panel, Fig. 2.1b**). The same concept was experimentally demonstrated using food color dyes (**Fig. 2.1c**).

Because of the laminar flow, turbulence is effectively eliminated, and the dominant mechanism of mixing in the chip is diffusion. The relatively high diffusion coefficients of small creatinine molecules and the Jaffe reagent result in their rapid, complete mixing within just a few millimeters in the mixing channel passing the T-junction (**Fig. 2.1b-c**). Upon complete mixing, the approximately 62 mm long reaction channel allows the mixture to significantly react for ~4 min at the linear flow speed of ~0.25 mm/s before the reacted mixture reaches the OW.

Because the mixing ratio between two laminar flows relies solely on their relative flow rates in the inlet channels, it is critical to maintain identical pressure in the sample and reagent inlet wells. Therefore, we applied our previously established 2-PPC technique for

pressure balancing[20]. Specifically, this is achieved by covering the sample and the reagent in the aqueous phase in the inlet wells with a single shared volume of silicone oil so that any pressure difference due to solution height variation in the wells is compensated by the immiscible oil phase coverage with similar mass density to the aqueous solution.

The color signal from the uCR-Chip is imaged and analyzed by an in-house developed imaging platform (**Fig. 2.1d**). The platform was configured with a white LED backlight panel, a chip-holding stage, and a USB microscope with a bandpass blue filter (wavelength peak at 490 nm) to record the colorimetric signal at the target optical absorbance wavelength from the OW in the uCR-Chip. The captured images were then transferred to a laptop computer for analysis. Together, the standalone passive microfluidic device with accurate mixing and reaction controls and the portable, low-cost imager provide a complete PoC creatinine test prototype.

2.3.2 Dry film photolithography for accurate microfluidic chip fabrication

Due to the absence of active external control, the functionality and performance of passive microfluidic systems highly depend on the specific geometric properties of the channels, especially for time-sensitive chemical reactions (**Fig. 2.2a**). Therefore, the accuracy and repeatability of the device fabrication are critical. SU-8 is a commonly used liquid photoresist for microfluidic device master mold fabrication[23–25]. Its various series of products can pattern a range of thicknesses on the substrate depending on the photoresist properties (e.g., viscosity) and the spin coating parameters. However, for more viscous SU-8 required to fabricate relatively thick patterns (e.g., SU-8 2075), spin-coating often results in considerable variation of pattern thickness. During the test we found that spin coating SU-8 resulted in up to ±20 μm variation, while the dry film photoresist resulted in only <1 μm

variation (**Fig. 2.2b**). Consequently, the variation in channel thickness leads to a cascade of changes in hydraulic resistance, linear flow speed, reaction time, and reaction signal (**Fig. 2.2c-f**). Therefore, we chose a dry film photoresist of pre-defined thickness for master mold fabrication. A more detailed analysis of the effect of channel thickness variation on uCR-Chip is available in the Supplementary Information (**Table 2.S1**).

2.3.3 Optimization of signal observation window geometry

To achieve effective absorbance-based colorimetric signal detection in the uCR-Chip using a portable imaging platform, the OW must be sufficiently large (e.g., millimeter scale) to ensure enough pixels for accurate color measurement. However, a larger OW with a simple geometry (e.g., a square shape) will require a longer filling time for the reacting mixture and is likely to create a nonuniform flow velocity profile, which complicates the distribution of the absorbance signal due to its dependence on reaction time. In this context, we hypothesized that optimizing the OW geometry could be one of the strategies to achieve a shorter OW filling time and a more uniform flow velocity profile in the OW. We designed, simulated, and tested different OW geometries (e.g., simple square, lenticular with or without a flow diverter, etc.), which helped us to select a more suitable OW design. Among these OW designs, we found the lenticular-shaped OW with a flow diverter optimizes the flow filling time and velocity profile. For example, it takes ~60 s to fill the lenticular + diverter OW by passive flows in the uCR-Chip compared to ~90 s to fill the simple square shape OW of similar size (**Fig. 2.3a**).

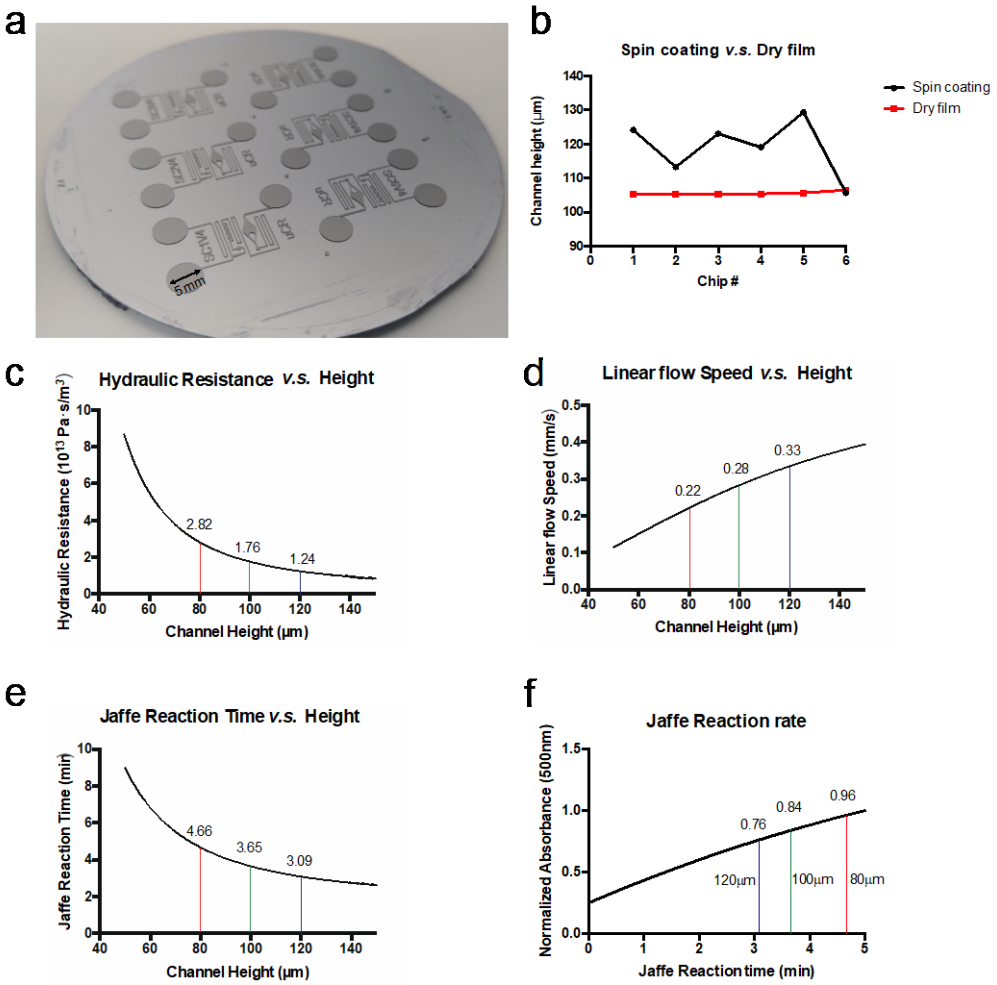

Figure 2.2 Comparison of the uCR-Chip fabricated by spin-coating and dry film photolithography

a. Photograph of the chip master fabricated by dry film photolithography on a silicon wafer, which includes six identical units; **b.** Comparison of the patterned photoresist thickness fabricated with dry film or SU-8 spin coating for 6 different chips. The spin-coated SU-8 2075 results in considerable pattern thickness variation (or equivalently, channel height variation) among different chips. The dry film fabrication yields near-identical channel height among different chips. **c-f.** Demonstration of the effect of channel height variation on the Jaffe reaction in a 60 mm long and 100 μm wide passive flow microfluidic channel. For example, the spin-coating of SU-8 2075 can lead to up to a 20 μm channel height deviation, which translates to approximately a 30% to 60% variation in hydraulic resistance relative to the desired 100 μm channel height (**c**). Subsequently, the hydraulic resistance variation could lead to variation of linear flow speed (**d**), which ultimately affects the reaction time (**e**) before the mixture enters the OW and therefore variation of the reaction signal in the OW (**f**). The reaction time t is mapped to the time-dependent reaction signal S up to 8 min from the 20 mM creatinine sample in the well-plate assay (**Fig. 2.4d**) (nonlinear fitting function: $S = -0.00669t^2 + 0.1529t + 0.1972$; $R^2 = 0.9982$). The signal is normalized to the 8 min signal.

Furthermore, COMSOL modeling shows that a lenticular + diverter OW produces a more uniform flow velocity across the width of the OW perpendicular to the flow direction (**Fig. 2.3b-d**). We reasoned that the lenticular OW design produces a more gradual flow transition from the narrow reaction channel to the wider OW, which helps stabilize the flow. The inclusion of a flow-diverting pillar at the entrance further enhances the uniformity by directing the flow closer to the OW walls and away from the center, compensating for the parabolic flow speed profile in a simple straight microfluidic channel. Thus, the lenticular + diverter OW design was chosen for the subsequent technical characterizations and validation of the uCR-Chip.

2.3.4 Technical characterizations of uCR-Chip

To characterize the technical performance of the uCR-Chip, we followed our established test protocol to measure the colorimetric responses of the Jaffe assay for a range of creatinine standard concentrations in a simple buffer up to 40 mM (**Fig. 2.4a**). For each creatinine concentration, we captured time series data of the detection signal from the uCR-Chip. Our results showed that the signal increases over time and reaches a plateau within 7 min after loading the sample, reagent and applying oil coverage (**Fig. 2.4c**). The plateau mainly results from the hydrodynamic equilibrium of flows in the channels and the OW, and the level of the plateau is proportional to the creatinine concentration, as expected (**Fig. 2.4c**). The 7 min signal stabilization reflects the time for mixing, reaction, OW filling, and flow stabilization. After 7 min, both the uniform color signal in the OW and the color gradient along the reaction channel remain stable. We showed the signal stability duration up to 3 min in the plot (**Fig. 2.4c**) and >30 min in the complete video recording.

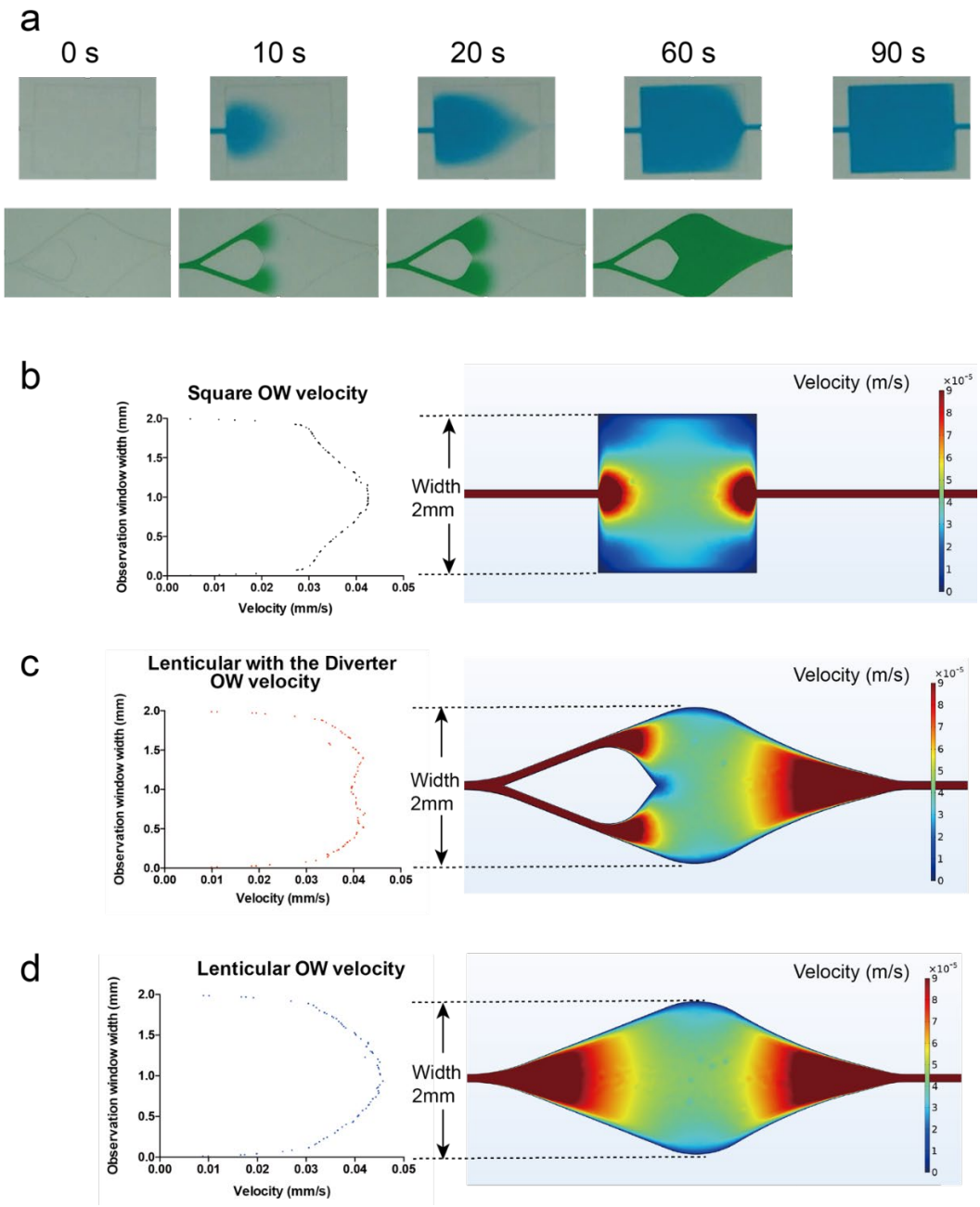

Figure 2.3 Optimization of signal observation window geometry

a. Effect of the OW geometry on OW filling time. The filling time of a typical square-shaped OW is around 90 s, while the lenticular with diverter OW geometry allows for <60 s filling time. As the food dye flows into the OW, the pre-filled water generates resistance as it is being displaced, which produces a diffusion front allowing observation of the OW filling dynamics; **b.** COMSOL simulation of the flow velocity profile in the uCR-Chip with a square OW shape; **c-d.** COMSOL simulation of the flow velocity profile in the uCR-Chip that has a lenticular OW with (**c**) or without (**d**) a diverter. The lenticular OW with a diverter shows a more uniform flow velocity in the center region of the OW compared to the square OW or the lenticular OW without a diverter.

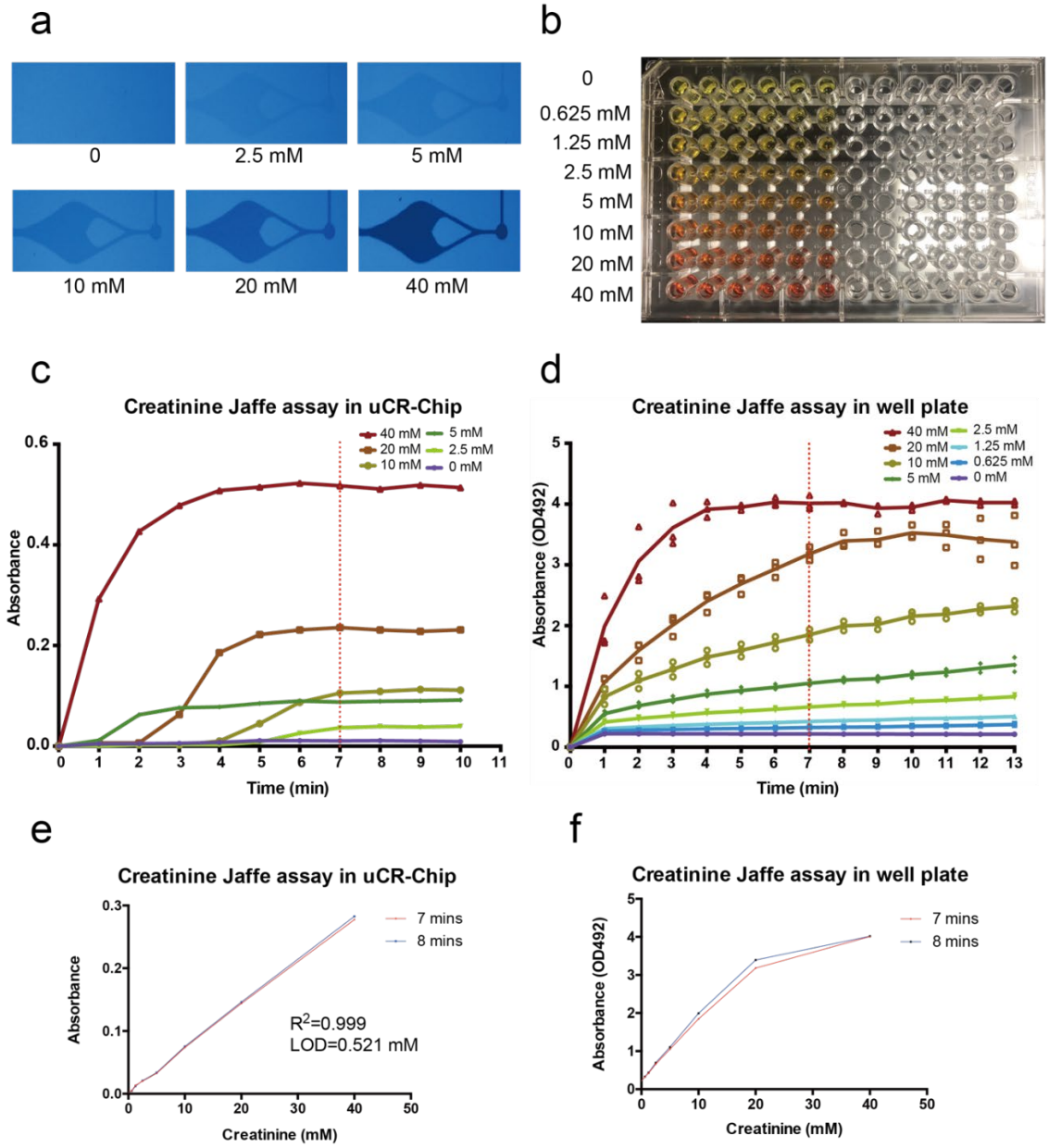

Figure 2.4 Technical characterizations of the uCR-Chip

a-b. The colorimetric responses of the Jaffe reaction of different concentrations of creatinine standard up to 40 mM spiked in simple buffer as visualized in the uCR-Chip (**a**) or the well plate (**b**); **c**. The Jaffe reaction signal stabilizes around 7 min for different creatinine concentrations in the uCR-Chip; **d.** By comparison, the signal does not stabilize for most creatinine concentrations in the well plate assay; **e-f.** Calibration curve for the uCR-Chip test (based on a separate set of experiments) shows stable linear responses up to 40 mM creatinine with a LOD of 0.521 mM (**e).** in comparison to the narrower linear range and unstable calibration curve in the well plate assay (**f**).

This signal stability offers a unique practical advantage for time-insensitive signal readout after 7 min of the assay in the uCR-Chip, which is particularly useful for PoC testing by the end users. Based on the time-series characterizations and signal stability results, we next repeated the tests and produced the calibration curve using the signal measurements at 7 min and 8 min (**Fig. 2.4e**). The results demonstrated a linear detection range up to 40 mM and a lower LOD of 0.521 mM (**Fig. 2.4e**), which covers the entire clinical urine creatinine concentration range. Identical calibration curves at the two time points consistently confirmed signal stability (**Fig. 2.4e**). As a reference method, we performed the same Jaffe assay using the standard 96-well plate and a commercial plate reader for absorbance measurement (**Fig. 2.4b**). Compared to the uCR-Chip, although the well-plate assay produced a clinically applicable calibration curve (**Fig. 2.4f**), the detection signal could not stabilize even at 13 min (**Fig. 2.4d**), consistent with previous reports from the literature[21,26]. At 7 min, the linear detection range of the well-plate assay is limited to 20 mM and the LOD > 0.6 mM, and the calibration curve at 8 min considerably deviates from the 7 min calibration curve; this trend would be expected to persist over a longer time period (**Fig. 2.4f**). Collectively, the uCR-Chip exhibited superior technical performance compared to the conventional test method and met the clinical detection range and sensitivity requirements for clinical use.

2.3.5 Technical validation of uCR-Chip using artificial urine

Based on the successful technical characterizations of the uCR-Chip, it is necessary to validate its effective use for testing urine samples. Technical validation of the uCR-Chip was performed using artificial urine for simplicity, better experimental control, and to mimic the physiological matrix. The preliminary clinical sample tests data is available in

Supplementary Information (**Fig. 2.S4**). Specifically, creatinine standards of different concentrations (i.e., 2.5, 5, 10 and 25 mM) were spiked into commercial artificial urine. The spiked samples were then tested in the uCR-Chip, and the full uCR-Chip calibration curve was used to predict the creatinine concentration in each sample. For comparison, the same batch of spiked samples was measured using a commercial benchtop PoC urine creatinine test (i.e., the Siemens DCA Vantage® test). The creatinine concentrations predicted by the uCR-Chip and the DCA test were compared with the theoretical concentrations of the spiked creatinine to evaluate recovery rate. Our results showed the expected linear correlation of the uCR-Chip predictions with the theoretical concentrations under the commonly accepted recovery rate range (i.e., 87-110% in our data) (**Fig. 2.5a-b**). Furthermore, the uCR-Chip showed a negligible base signal for the blank artificial urine sample. By contrast, the DCA test predicted a significant base creatinine concentration (4.4 mM) in the blank artificial urine control sample, suggesting its sensitivity to the matrix effect. However, upon calibration by deducting the base creatinine concentration, the DCA test predictions were more closely correlated with the theoretical concentrations and yielded a higher recovery rate (i.e., 96-104%) (**Fig. 2.5a&c**). Consistently, the predictions of the spiked creatinine concentrations by the uCR-Chip and the DCA test are correlated (**Fig. 2.5d**). Thus, the uCR-Chip was successfully validated using the artificial urine and demonstrated comparable or even better performance than the commercial PoC test.

2.4 Discussion

Although microfluidic devices have been increasingly developed for renal disease diagnostic applications[16], they are not yet used in current commercial PoC urine creatinine tests. Urine dipstick tests such as the Siemens Multistix® are easy to use and inexpensive but are limited to qualitative or semi-quantitative test results and suffer from poor sensitivity and low accuracy. In comparison, sophisticated benchtop test systems such as the Abbott Afinion™ and the Siemens DCA Vantage® tests produce more reliable and quantitative analytical results. However, these tests require bulky, expensive, and complicated analyzers, making them non-ideal for mobile clinics, resource-limited and remote regions, or personal use. In this context, the microfluidics-based uCR-Chip balances the pros and cons of the existing tests and demonstrates its promise to enable practical urine creatinine measurement at PoC (**Table 2.S2**). Our uCR-Chip is very easy to operate, requiring simple loading steps by the users; has a low chip material cost of under $1 US dollar per test; and the detection signal can be conveniently read by a portable and lightweight imager assembled using affordable off-the-shelf parts. At the same time, it provides fully quantitative test results with detection sensitivity, range, and speed comparable to or even better than the commercial benchtop systems and offers the unique advantage of signal stability (**Table 2.S2**). Other types of microfluidic tools for biomedical detection include, but are not limited to, paper-based and centrifugal microfluidic platforms. For example, paper-based chips have emerged as a useful platform for rapid, easy-to-use, high-throughput, and low-cost biochemical detection[27-28]. However, these devices are often limited by test accuracy, so they are primarily used as qualitative or semi-quantitative screening tools. On the other hand, centrifugal microfluidics utilizes centrifugal force to enable flexible fluid manipulation for rapid sample

isolation and automated biochemical reactions[29]. However, this class of microfluidic devices is not well-suited for applications requiring continuous flow mixing, and it typically needs a special external spinning instrument, which is not ideal for PoC diagnostic applications outside research labs. In contrast, the passive-flow microfluidics approach used in the uCR-Chip enables true quantitative and accurate diagnostic testing while remaining relatively easy to use due to its standalone operation. Much of the innovation in this work focuses on developing methodologies to reduce the operational skill requirements while maintaining test accuracy.

Traditionally, miniaturized microfluidic devices are powered and operated by specialized external equipment such as pumps and valves[30–33]. Various on-chip actuation strategies, such as elastic membrane valves and pumps[34–37] or electrode arrays[38,39], enable more flexible active fluid manipulations and create large-scale, integrated, and programmable microfluidic circuits[40,41]. However, these devices still require external power or pressure sources as well as an electronic control system[42–45], limiting them to laboratory research. For practical PoC diagnostic applications, unless the entire microfluidic system, including both the chip and the active control system, can be miniaturized, passive microfluidic devices offer some clear advantages derived from their intrinsic features of being standalone, self-operated, and external equipment-free[46–50]. The common drawback of the passive microfluidic approach is its high susceptibility to variations in device parameters and experimental conditions due to a lack of active controls, which results in accuracy and reliability concerns. In this context, the design and operation strategies used in the uCR-Chip test, including **1)** accurate microfluidic channel fabrication by dry film lithography, **2)** robust mixing and reaction control by the combination of the oil-coverage-based 2-PPC technique

and microfluidic channel network design, **3)** flexible detection signal readout time enabled by continuous-flow-based fast signal stabilization without requiring reaction equilibrium, and **4)** rapid iterative device design prototyping and optimization, provide some useful reference guidelines to develop passive microfluidic devices, especially for end-user-oriented PoC diagnostic applications.

The viscosity of the reagents is a crucial factor to consider when designing a passive microfluidic system. More specifically, both the flow rate and diffusion properties of the fluid depend on viscosity, which affects fluid transport and mixing. However, in the case of the uCR-Chip, all the solutions involved in the test, including the Jaffe reagent, the creatinine standard, the artificial urine, and real urine samples, are highly diluted fluids; therefore, their viscosity is close to that of water. Consistent with this assumption, we did not observe different flow rates for these solutions in the same microfluidic channel under the same hydrostatic pressure difference between the inlet and outlet. Thus, the differential flow rate-based mixing ratio control and the diffusion-dominated fluid mixing in the uCR-Chip can be readily modeled using known physics under the assumption of viscosity identical to that of water for all solutions. However, if the sample appears to be more viscous, which is possible for some patients' urine samples, proper dilution will be required before testing so the differential viscosity effect on flow and mixing can be minimized.

a

Spiked samples Conc. (mM)	uCR-Chip prediction (mM)	uCR-Chip recov. %	DCA (mM)	DCA recov. %
2.5	2.759	110	2.40	96
5	5.441	109	4.90	98
10	10.336	103	10.30	103
25	21.797	87	26.10	104

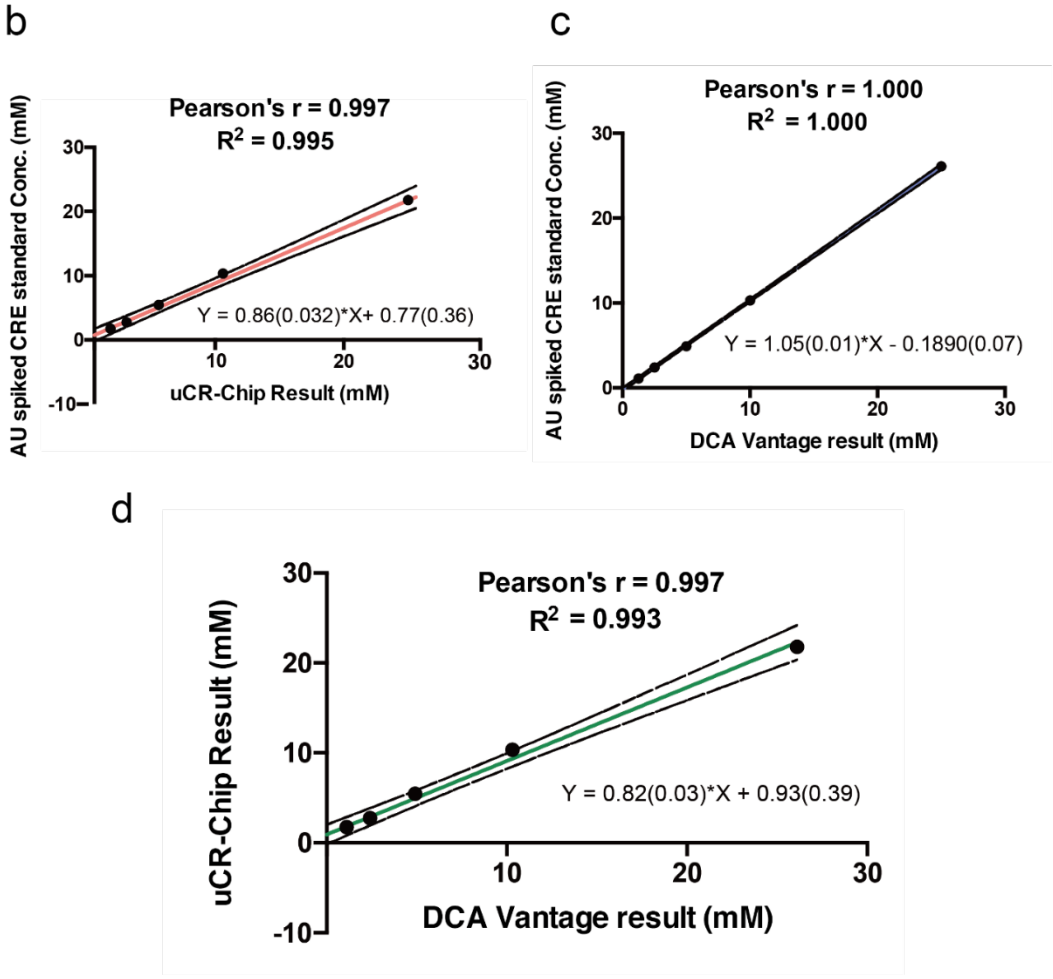

Figure 2.5 Technical validation of the uCR-Chip using artificial urine

a. The summary table of the theoretical creatinine standard concentrations spiked in artificial urine, their predictions by the uCR-Chip and the DCA Vantage test, and their respective percentage recovery. **b.** The correlation plot between the uCR-Chip test prediction and the theoretical creatinine concentrations; **c.** The correlation plot between the DCA Vantage test prediction and the theoretical creatinine concentrations; **d.** The correlation plot between the DCA Vantage test prediction and the uCR-Chip test prediction. Pearson's *r*, R^2 and the linear fit functions (the number inside the bracket is the standard error of the respective fitting parameter) are shown for **b-d.**

The native urine color can potentially present a spectral interference with the Jaffe reaction signal. In this regard, several aspects of chip design could mitigate this effect and some preliminary research efforts to address this issue. **First**, in our technical validation studies, we spiked creatinine standard in artificial urine, which mimics the real urine properties, including its native color. Our results showed an acceptable recovery rate (**Fig. 2.5a**), suggesting the urine color itself is not significantly interfering with the Jaffe reaction color signal in the uCR-Chip. **Second**, the urine sample is mixed with Jaffe reagent at the 1:5 ratio, so the urine is considerably diluted, which helps reduce its native color spectral interference. To further reduce this spectral interface, the urine sample can be pre-diluted in buffer before adding to the uCR-Chip for mixing and reaction with the Jaffe reagent. However, this dilution strategy will require higher detection sensitivity, and we discuss some possible approaches to achieve it in the Discussion section. **Third and finally**, we have developed a new proof-of-concept prototype of the uCR-Chip that allows measurements of the Jaffe reaction kinetics through multiple serially located OW along the reaction channels (we called it the "kinetic uCR-Chip" or "K_uCR-Chip" due to its kinetics measurement feature or the "uCR-Abacus Chip" based on the similarity of the chip design's graphical look to an abacus). In this new chip, the Jaffe reaction color signal over time can be measured over the OW series (**Fig. 2.S3**). Thus, the relative color signal change is measured instead of the absolute color signal, which effectively eliminates the background urine color spectra interference. In similar consideration, the uCR-Chip can be modified to include an initial reference OW along the Jaffe reagent inlet channel for background color subtraction.

Previously, we successfully developed a passive microfluidic device for rapid measurement of urinary albumin (uAL-Chip)[20]. The uAL-Chip development established the

core chip design and operation principles for our passive microfluidic devices. It utilizes the Albumin Blue probe to produce a highly sensitive and specific fluorescent signal upon reacting with urine albumin, covering the full clinically relevant concentration range for quantitative categorization of albuminuria. However, albuminuria classification by urine albumin alone is inaccurate, requiring calibration by urine creatinine to determine uACR[51,52]. Thus, it is desirable to design a similar passive microfluidic device for urine creatinine measurement that can be readily integrated with the uAL-Chip. A practical challenge of this approach is the lack of a reliable one-step reacting fluorescent probe for detecting creatinine. As such, in the current uCR-Chip development, we chose the traditional Jaffe reaction for colorimetric quantitation of urine creatinine as a proof-of-concept bearing its known limitations[21,22]. Our envisioned dual urine marker chip will be designed to have a common sample loading inlet, which will be split and directed to interface with the uAL-Chip and uCR-Chip units for albumin and creatinine measurement, respectively, all on a single device. The 2-PPC technique can be consistently applied to the chip by covering all inlets with a common drop of silicone oil. Thus, an integrated solution for uACR determination based on a passive microfluidic device can be realized (uACR-Chip). To detect signals from the uACR-Chip, a dual-module portable imager capable of reading fluorescent and colorimetric signals is required for the chip's practical use. The preliminary uACR-Chip prototype design and testing are provided in the Supplementary Information (**Fig. 2.S2**). On the other hand, incorporating multi-stage mixing into the uCR-Chip will permit the more advanced enzymatic creatinine assay. The enzymatic method can be compatible with fluorescent detection signal readout and improves detection specificity, which is one of the known issues of the Jaffe assay due to positive interference with Jaffe-like chromogens. Such a multi-stage

mixing approach would also facilitate the use of any other additives required for on-chip mixing control, such as the nonionic surfactant Tween-20 in the current uCR-Chip test protocol.

Although the uCR-Chip has been successfully used to test creatinine standards spiked in artificial urine, validation with real urine samples from CKD patients is expected to further validate its clinical usability. To this end, we have conducted preliminary clinical sample tests, and the data are available in the Supplementary Information (**Fig. 2.S4**). Moving forward, to further clinical use of the device and automate the test, on-chip reagent storage and release-on-demand functions will be required, which can be adapted from established methods such as blister packs[53,54]. Considering the specificity issue of the Jaffe assay, samples from subjects that have abnormal endogenous Jaffe-like chromogens in urine, such as liver disease patients, jaundiced patients, and others (hemoglobinuria), would be excluded from the validation test using the current version of the uCR-Chip. With proper sample dilution (off-chip or on-chip), the uCR-Chip can predict higher creatinine concentrations in the naïve urine sample beyond the chip's current upper detection limit, although urine creatinine higher than 40 mM is clinically uncommon. On the other hand, CKD urine samples can present higher albumin concentrations and require dilution to fit the detection range of the uAL-Chip. Thus, the low LOD of the uCR-Chip allows consistent dilution of the urine sample up to two-fold without losing sensitivity. Further improving the sensitivity of the uCR-Chip would permit higher levels of sample dilution as needed and may ultimately enable detection of the much lower creatinine concentration in blood for eGFR determination[55]. In this regard, effectively increasing the optical path to enhance light absorbance without compromising sample-reagent mixing efficiency is required. Finally,

beyond CKD diagnosis, it is worth pointing out the broader biomedical relevance of urine creatinine measurement, such as monitoring athlete health, pregnancy, and drug abuse, which can all benefit from a PoC test enabled by the uCR-Chip.

2.5 Materials and methods

2.5.1 Materials

The uCR-Chip design pattern was printed using a Xerox wax printer (ColorQube 8870). A TOYO-VIEW 4×5 camera was used to image the chip design onto the photo film. Other materials used for photomask fabrication include the photo film (Arista Ortho Litho Film 3.0-4×5), the photo developer (Arista Powder A&B Litho Developer), the photo film fixer (Ilford Rapid Fixer) and the washing solution (Kodak Photo-Flo 200). The SUEX dry film photoresist was purchased from MicroLaminates (Sudbury, MA, USA), and the 3-inch silicon wafer was ordered from Silicon Inc. (Plano, TX, USA). Dow SYLGARD™ 184 Silicone Elastomer Clear was purchased from Ellsworth Adhesives (Germantown, WI, USA). The DCA Vantage™ Analyzer and DCA® Microalbumin/Creatinine Urine Test were purchased from Siemens Medical Solutions Diagnostics (Tarrytown, NY, USA). The Jaffe assay reagents were purchased from Randox Laboratories (County Antrim, UK) and the traceable creatinine standard was purchased from Sigma Aldrich (Oakville, ON, Canada). Tween-20 was purchased from Sigma Aldrich (Oakville, ON, Canada). Silicone oil was purchased from Alfa Aesar (Ward Hill, MA, USA). The artificial urine (S07906) was purchased from Fisher Scientific (Ottawa, ON, Canada). Materials for the portable imaging system include a USB microscope (Dino-Lite Premier AD4113T, AnMo Electronics Corporation, New Taipei City, Taiwan), a blue bandpass filter (FB490-10-Ø1", THORLABS) and a white LED light panel (“Lumen”) from Hey Paparazzo (Ely,

Cambridgeshire, England). The Microplate Photometer (Multiskan FC) was from Thermo Scientific (Mississauga, ON, Canada).

2.5.2 Microfluidic chip design and modeling

The chip pattern was designed using AutoCAD (Ver. 2023). Laminar flow mixing in the uCR-Chip was modeled in COMSOL Multiphysics (Ver. 5.5). For creatinine, the diffusion coefficient was set approximately in the order of 10^{-5} cm^2/s[56]. Since the diffusion coefficient for the Jaffe reagent (i.e. picric acid and sodium hydroxide) is not directly available in literature to our best knowledge, we approximated it to be in the same order of 10^{-5} cm^2/s based on the considerations of **1)** known molecular weight of creatinine (~113 g/mol), picric acid (~229 g/mol), and sodium hydroxide (~39 g/mol); **2)** the general relationship between the hydrodynamic radius and molecular weight ($r \sim \text{molecular weight}^{1/3}$); and **3)** the general inverse proportionality between the diffusion coefficient (D) and the hydrodynamic radius ($D \sim 1/r$). The Reynolds number was calculated to be ~0.025 based on the simulated flow speed of ~0.25 mm/s inside the 100 μm high mixing channel and the fluid density and dynamic viscosity of $\sim 10^3$ kg/m^3 and $\sim 10^{-3}$ Pa·s respectively, ensuring the nature of laminar flow mixing in the uCR-Chip.

The inlet pressure was chosen to be 50 Pa, which represents approximately 5mm of water column pressure based on the reagent or sample volume added to the inlet wells and the inlet dimensions. The outlet pressure was set to zero based on the assumption of an empty well. Because the reagent/sample loading volume is much larger than the volume of the microfluidic channels and the flow rate is relatively low, the pressure difference between the inlets and outlet can be reasonably approximated to be a constant over the test period. The height of all microfluidic chip sections was set to 100 μm in the simulation. Guided by the

general inverted inlet channel length ratio to achieve the mixing ratio, the exact inlet channel length was fine-adjusted until the desired mixing ratio was achieved. Similarly, the mixing and reaction channel lengths were adjusted until complete mixing and the desired reaction time were achieved, respectively. The mixing ratio was simulated by setting the chemical concentration in the left inlet channel (short 1L) to 0 and the chemical concentration in the right inlet channel (long 5L) to unity (i.e., 1 mol/m³). Therefore, a 1:5 right-to-left flow mixing ratio produces approximately 0.166(6) mol/m³ upon complete mixing (**Fig. 2.1b**).

2.5.3 In-house photomask fabrication

The uCR-Chip photomask was fabricated in the lab using an optical reduction technique (**Fig. 2.S1**)[57]. The 9X size amplified chip design was printed as solid black patterns on a piece of printing paper using a wax printer (Xerox ColorQube 8870) for high-contrast imaging. The printed chip design was posted on a whiteboard in a well-lit room. Then the image was captured on a black-and-white Arista Ortho Litho Film 3.0 using a TOYO 4×5 film camera. The chosen film has a very low ISO of approximately 0.5 - 6, high resolution, and high contrast, which was further increased using the push-pull technique (www.kodak.com). Slightly underexposing the film helps keep the transparent regions clean, followed by over-developing to darken the rest of the film.

We used a 4 s exposure time and a 5 min developing time in 1 liter of developer. The developing solution was prepared following the manufacturer's instructions (www.freestylephoto.com). Immediately after developing, the film was rinsed in a 5% acetic acid bath (which can be replaced by citric acid) for 2 min to stop the developing process. Then the film was rinsed for another 4 min in a fixer bath (Ilford Rapid Fixer). Lastly, the film was treated with a final rinse in a water bath with 2-3 drops of wetting agent (Kodak

Photo-Flo 200 Solution) to minimize water marks and promote uniform drying. The developing and rinsing in stopper and fixer baths were done in a darkroom under a red safelight.

It is worth pointing out that exact timing for exposure and developing, as well as the amount of light, are generally important in film photography to obtain high-quality photos. On the other hand, preparing a high-contrast photomask for photolithography does not require precise reproduction of shades of gray. Specifically, for non-grayscale photomasks, the pattern on the photo film is either opaque (black) or transparent. The photo film has a logarithmic relationship between exposure time and optic density. Therefore, low-sensitivity film like the one used for our photomask fabrication is not sensitive to small variations in exposure time. This low time sensitivity is similar for film development, which overdevelops the opaque regions on the film while keeping the unexposed clear regions "untouched". In general, the level of gray (i.e. "gamma" as termed in photography) versus developing time will eventually reach a plateau or maximum density. Therefore, the exposure and development time used in our photomask fabrication was set to allow sufficient photo film overdevelopment and contrast without requiring high precision time control. In particular, the "Arista Ortho Litho 3.0" film used in our photomask fabrication is designed for high-contrast images. Collectively, these features of photo films enabled effective controls of our photomask fabrication method.

2.5.4 Microfluidic chip fabrication

The chip mold was patterned using a 100 μm thick SUEX dry film photoresist on a 3-inch silicon wafer following the standard dry film photolithography protocol[58] in the Nano Systems Fabrication Laboratory at the University of Manitoba. Then the photoresist pattern

was transferred to the polydimethylsiloxane (PDMS) replica using the standard soft-lithography method[59]. The PDMS replica of 5 mm thickness was cast from the mold, and 5 mm diameter holes were punched to serve as the inlet and outlet wells. A separate 2 mm thick blank PDMS slab with a rectangular-shaped hollow hole that matches the size of the inlet wells of the channel-containing PDMS replica was prepared separately. The two PDMS slabs were O_2 plasma bonded, with the rectangular hole of the blank PDMS aligned to the inlet wells of the channel-containing PDMS replica, such that oil coverage for the inlet wells is confined to a defined volume. Finally, the entire PDMS slab was air plasma bonded to a clean glass slide to seal the channels. The microfluidic channels and all the inlet and outlet wells were filled with DI H_2O immediately after plasma bonding to maintain hydrophilicity, and the chip was kept inside a clean bench until use, typically within the same day.

2.5.5 uCR-Chip test protocol

The Jaffe assay working solution was prepared according to the manufacturer's instructions. Specifically, R1 (1% picric acid) and R2 (0.75N NaOH) were mixed at a 1:1 ratio and the mixed working solution was immediately used to react with creatinine[21,22]. Tween-20 was added to the sample (creatinine standard spiked in DI H_2O, artificial urine, or real urine sample) and the working solution at the final concentration of 0.05% (V/V), which is required to prevent backflow at the mixing junction of the uCR-Chip by reducing surface tension in the current test protocol. Immediately before the test, water from inlet and outlet wells was emptied using a pipette. Then, the prepared sample and the working solution, each at approximately 60 μL volume, were loaded simultaneously using a multi-channel pipette. This was followed by adding a common drop of silicone oil to cover both inlets and fill the entire oil confinement reservoir so that the total solution height in the inlet wells is

consistently balanced. An original image of the OW before loading the reagents was taken as the chip's internal reference control (i.e., the 0^{th} minute image), and a second image of the OW was captured after 7 min (the 7^{th} minute image) using the USB microscope-based image platform. For the signal stability test, the images were recorded for a longer time at shorter time intervals. The acquired images were analyzed using ImageJ (Ver. 1.49v) to measure the average OW blue channel intensities I and I_0 for the 7^{th} minute image and the 0^{th} minute image, which were used to calculate transmittance T and absorbance A (**Eq. 3**). Following the Beer-Lambert law[60], absorbance A is directly proportional to the molar absorption coefficient $\boldsymbol{\varepsilon}$ of the particular substance, the molar concentration c, and the optical path length l. Thus, the absorbance linearly correlates with the concentration of the Janovsky complex and equivalently correlates with the creatinine concentration in the sample.

$$A = -\log_{10}(T) = -\log_{10}\left(\frac{I}{I_0}\right) = \varepsilon c l \qquad \textbf{Eq. 3}$$

2.5.6 Creatinine Jaffe assay in well-plate

The Jaffe assay was conducted in the well plate according to the manufacturer's instructions. R1 (1% picric acid) and R2 (0.75N NaOH) were mixed at a 1:1 ratio, and the mixed working solution (25 µL R1 mixed with 25 µL R2 for each reaction) was immediately used to react with the creatinine standard sample (5 µL). Tween-20 was added to the sample (creatinine standards of 0.625, 1.25, 2.5, 5, 10, 20 and 40 mM prepared in DI H_2O) and the working solution at a final concentration of 0.05% (V/V) to be consistent with the uCR-Chip testing. The absorbance value (O.D. at 492 nm) of each reaction in the 96-well plate was measured by a plate reader at different time points up to 13 min.

2.5.7 DCA Vantage® ACR test protocol

The DCA Vantage® ACR test (in which the creatinine test is based on the Benedict-Behre reaction) was used as a commercial PoC creatinine test for comparison with the uCR-Chip test. The DCA test was conducted using the test cartridge from the kit and the DCA Vantage analyzer following the manufacturer's instructions. The tip of the capillary tube was inserted into the creatinine standard sample (approximately 100 µL per sample; four sample groups: 2.5, 5, 10, and 25 mM creatinine spiked in the commercial artificial urine) up to the level above the starch plug. The capillary holder was then secured into the cartridge until it snapped into place. Subsequently, the cartridge was inserted into the analyzer system, the plunger was depressed into the cartridge, the flexible pull-tab was removed, and the compartment door was closed to initiate the assay within the analyzer.

2.5.8 Data analysis

Statistical analysis was performed using GraphPad Prism 6.0. Each individual test was repeated at least 3 times. The detection signal data and the creatinine concentrations were linearly interpolated to produce the calibration curves. The linearity of the regression was evaluated by the coefficient of determination R^2. The LOD was calculated using the standard method from the linear regression.

$$LOD = 3 \cdot \left(\frac{\sigma}{s}\right) \qquad \textbf{Eq. 4}$$

where σ is the standard deviation of the regression intercept and s is the regression slope respectively.

For the validation test using creatinine standard spiked in artificial urine, the recovery rate was calculated as (experimental prediction ÷ theoretical value) × 100%. The Pearson's

correlation coefficient *r* was applied to quantify the linear correlation between two sets of data.

2.6 Supplementary Information

2.6.1 Preliminary clinical samples test with uCR-Chip

The study protocol was approved by the University of Manitoba Human Research Ethics Board and the Seven Oaks Hospital Health Research Review Board. Under the informed consent, urine samples from CKD patients were collected at the Seven Oaks General Hospital in Winnipeg. Following the protocol in the Method section of the manuscript, we measured the creatinine level in the 10 CKD urine samples using both the uCR-Chip and the commercial DCA test (**Fig. 2.S4a**). The clinical standard Deming regression and the conventional linear regression as part of a specialized software package (EP Evaluator) are applied for the comparison analysis, and the preliminary results showed relatively comparable test data between the uCR-Chip and the DCA test (**Fig. 2.S4b**).

2.6.2 Comparison of microfluidic device fabricated by dry film photolithography vs SU-8 spin-coating based photolithography for uCR-Chip test

To demonstrate the importance of microfluidic channel fabrication accuracy for the uCR-Chip test, we provide a brief analysis of the effects caused by channel height variations. In the example discussed in this section, we consider a single microfluidic channel with a fixed length, width, and hydrostatic pressure difference between the inlet and outlet.

Assuming the microfluidic reaction channel has a length and width of 62 mm and 100 μm, respectively, a 20 μm channel height variation leads to a significant variation in hydraulic resistance (**Table 2.S2**). Considering the entire microfluidic channel network and OW of the uCR-Chip, the hydraulic resistance variation can be even more pronounced, depending on

the exact design. Further, with a hydrostatic pressure difference of 50 Pa between the inlets and outlet (i.e., ~5 mm water column pressure), the hydraulic resistance variation alters the linear flow speed, which in turn affects the Jaffe reaction time before the mixture reaches the OW, assuming complete mixing at the beginning of the reaction channel.

Consequently, since the Jaffe reaction signal remains in the rising phase at the end of the reaction channel (as a longer channel would extend the test time beyond the desired rapid PoC test and is not necessary for accurate quantification), variations in reaction time lead to different absorbance signal measurements in the OW. Altogether, this simplified calculation demonstrates the importance of channel height accuracy for the uCR-Chip and supports the usefulness of dry film mold fabrication. Although not directly addressed here, dry film mold fabrication is reasonably predicted to achieve better channel thickness uniformity across the chip than spin-coating SU-8, thus improving accuracy and consistency in the reaction signal. Therefore, the use of dry film photolithography is critical to ensuring the reliability and repeatability of uCR-Chip tests.

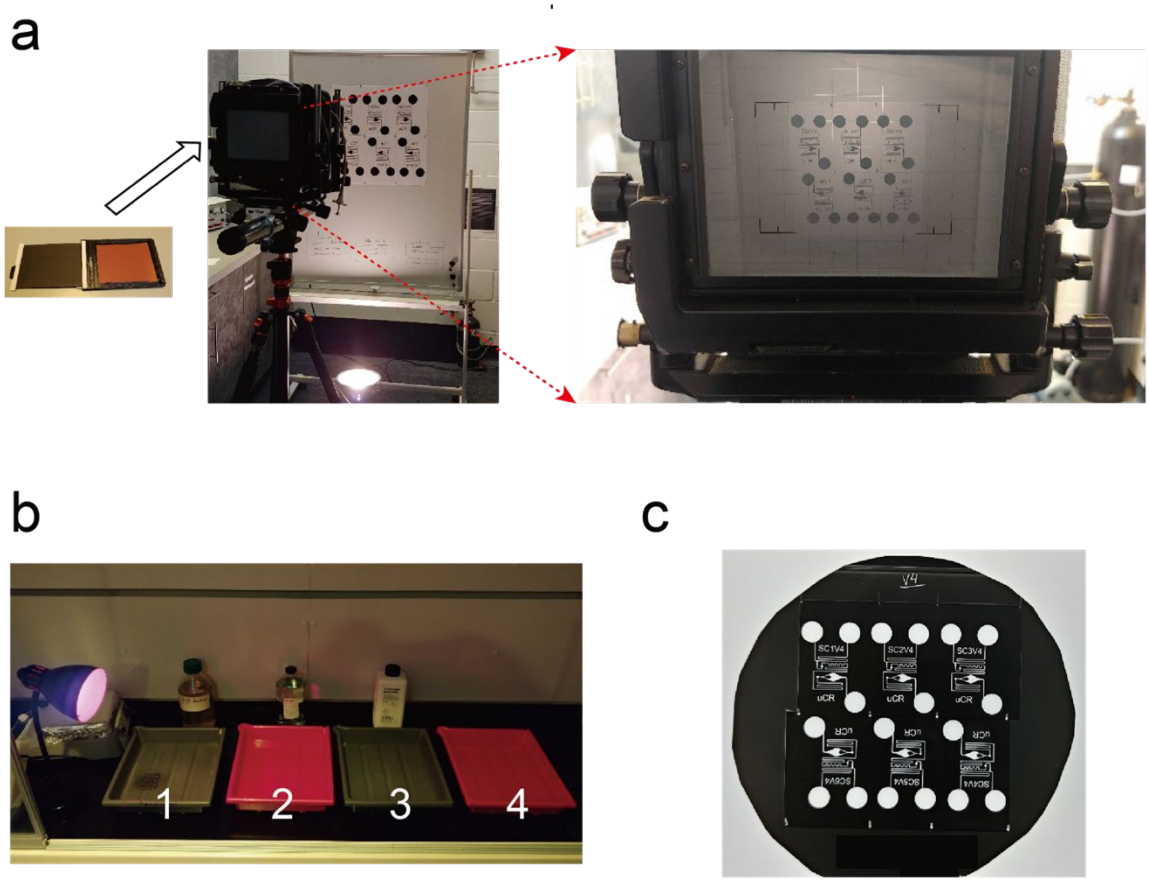

Figure 2.S1 Illustration of the in-house uCR-Chip photomask fabrication method

a. Illustration of the photomask imaging. The design pattern of the uCR-Chip was printed onto printing paper using a wax printer for high-contrast imaging. The printout was attached to a whiteboard using small magnets. For imaging, the film was loaded into the film frame, which was then installed in the camera. The distance from the camera to the board depends on the optics and the reduction scale of the printed design pattern to the photomask film. In our case, the distance is ~140 cm – 180 cm (~55" – 70") and the scale is ~9:1. Once the film was exposed, the film frame cover was put back and the film frame was stored until ready for developing. **b.** Illustration of the film developing steps. The film developing was done in 4 trays in sequence. Tray 1 is filled with the developer (1:1 mix of parts A and B). The developing time is 5.5 min. Tray 2 is filled with vinegar (stopper) that stops the action of the developer. Two minutes in the stopper is generally enough to stop the reaction. Tray 3 is filled with the fixer solution to fix the developed pattern on the film. Four minutes of soaking is typically sufficient. Tray 4 is filled with water with a drop of surfactant (Kodak Photo-Flo). This step makes sure that the film is clean and dries without stains. **c.** Picture of a finished uCR-Chip photomask.

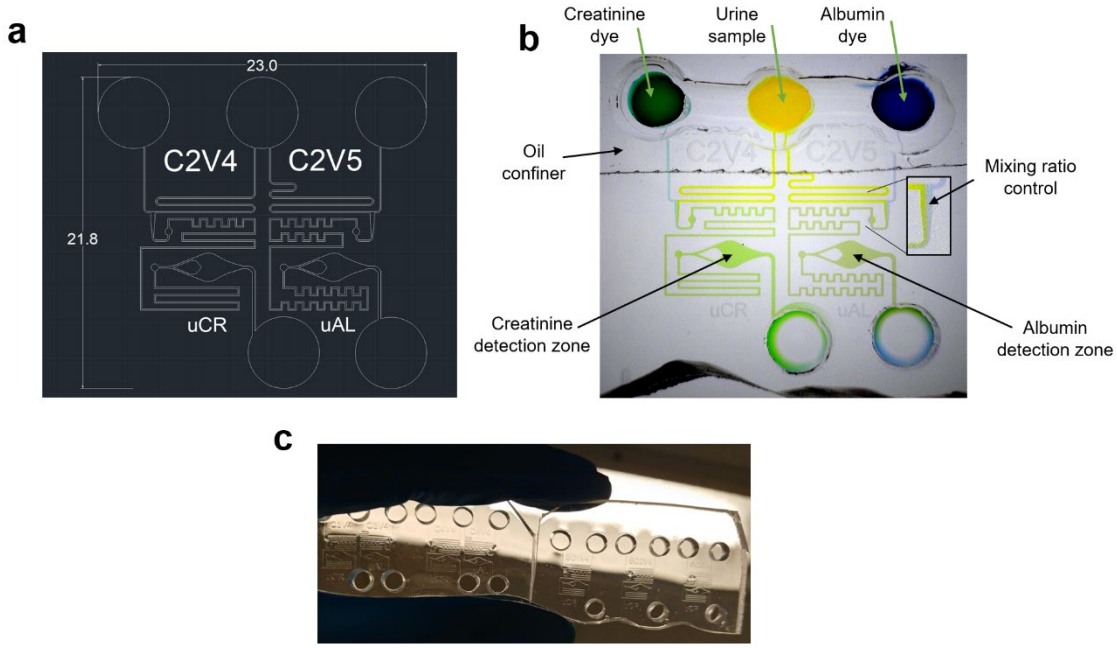

Figure 2.S2 Demonstration of the dual urine albumin and creatinine test chip

a. The schematic design of the integrated dual urine markers test chip. Dimension labels are in millimeters. **b.** Demonstration of the integrated chip test using food color dyes to mimic mixing and reaction. **c.** Example of the integrated dual-makers test chip (left; 2 units per chip) and the single-marker test chip (right; 3 units per chip). Labels of different combinations of letters and numbers are for practical labeling of the chip designs only.

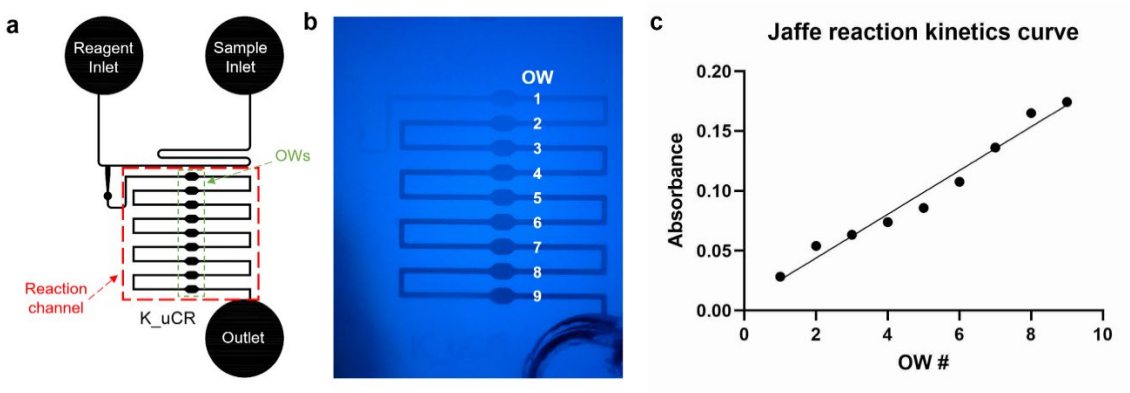

Figure 2.S3 uCR-Abacus Chip for measuring Jaffe reaction kinetics

a. The schematic design of the uCR-Abacus Chip; **b.** Example image of the Jaffe reaction in the uCR-Abacus Chip, where the darkness of the color signal over the OW series is demonstrated; **c.** Plot of the color signal intensity vs. OW number of the uCR-Abacus Chip in (**b**).

a

Sample ID	DCA reading (mM)	uCR-Chip reading (mM)
1	2.8	3.1
2	9.9	11.3
3	6.3	6.1
4	7.6	7.6
5	15.5	14.9
6	7	10.8
7	2.5	3.9
8	10.8	7.8
9	8.2	13.5
10	1.9	4.7

b

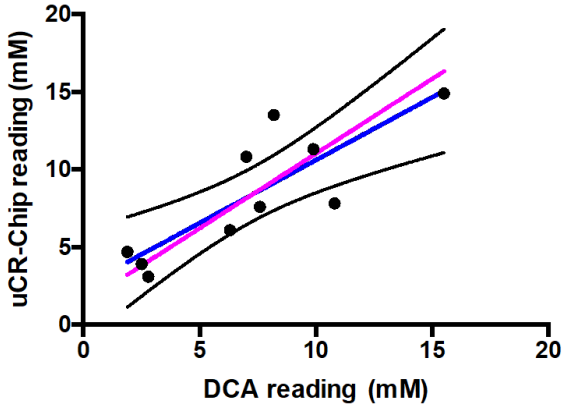

Figure 2.S4 Preliminary validation of the uCR-Chip test with 10 clinical urine samples from CKD patients

a. Comparison of the uCR-Chip test data with the commercial DCA creatinine test data of the 10 CKD urine samples. **b.** The clinical standard Deming regression and conventional linear regression are applied to compare the uCR-Chip test and the DCA test of the 10 CKD urine samples. The blue line shows linear regression and the pink line shows Deming regression ($R^2 = 0.84$). The black dashed lines indicate the 95% confidence intervals for the linear regression. In addition, the data was analyzed by specialized software, EP Evaluator (which consistently applies the Deming regression and linear regression for comparison analysis), and the result shows that the uCR-Chip is considered an alternative quantitative method to the DCA method. Furthermore, the paired *t*-test gives the *p* value of 0.17, indicating no statistically significant difference between the uCR-Chip test and the DCA test.

	Detection assays	Reaction assay	Detection type	Sample volume	User skill level	LOD	Detection range	Detection speed	Cost (US dollars)	Signal stability
Dipstick strips	Siemens Clinitek® Microalbumin Reagent Test Strip	Jaffe method	semi-quantitative	~20 µL	Low	0.884 mmol/L	0.884-26.520 mmol/L	Fast (<5 min)	~$1.46/each strip[1]	a few minutes to an hour
Afinion™ ACR	Enzymatic	proprietary	quantitative	3.5 µL	Medium	1.449 mmol/L	1.449-30.056 mmol/L	Fast (<5 min)	$10.5/each cartridge[2]	up to 10 minutes
DCA Vantage	Colorimetric	benedict-behre chemistry	quantitative	40 µL	Medium	1.3 mmol/L	1.3-44.2 mmol/L	Fair (5-10 min)	$4.8/each cartridge[3]	up to 90 minutes
Minuteful kidney test	Colorimetric	Peroxidase-like activity of copper creatinine complex	semi-quantitative	~20 µL	Low	0.884 mmol/L	0.884-26.520 mmol/L	Fast (3-5 min)	$6.38/each cartridge[4]	a few minutes to an hour
uCreatinine Chip	Colorimetric	Jaffe method	quantitative	50-60 µL	Low	0.521mmol/L	0.625-40 mmol/L	Fair (8-10 min)	~$0.87/each test	at least 30 mins

Table 2.S1 Comparison of the uCR-Chip with selected commercial PoC urine creatinine tests

2.7 References

1. Charles, C. & Ferris, A. H. "*Chronic Kidney Disease".* **Primary Care: Clinics in Office Practice** 47, 585–595 (2020).
2. Francis, A., Harhay, M.N., Ong, A.C.M., *et al. "Chronic kidney disease and the global public health agenda: an international consensus".* **Nat Rev Nephrol** 20, 473–485 (2024).
3. Jager, K. J., Kovesdy, C., Langham, R., *et al. "A single number for advocacy and communication—worldwide more than 850 million individuals have kidney diseases".* **Nephrology Dialysis Transplantation** 34, 1803–1805 (2019).
4. Bello, A. K., Okpechi, I.G., Levin, A., *et al. "An update on the global disparities in kidney disease burden and care across world countries and regions".* ***Lancet Glob Health*** 12, e382–e395 (2024).
5. Kovesdy, C. P. *"Epidemiology of chronic kidney disease: an update 2022"*. **Kidney Int Suppl** (2011) 12, 7–11 (2022).
6. Ndumele, C. E., Rangaswami, J., Chow, S.L., *et al. "Cardiovascular-Kidney-Metabolic Health: A Presidential Advisory From the American Heart Association".* **Circulation** 148, 1606–1635 (2023).
7. Jankowski, J., Floege, J., Fliser, D., Böhm, M. & Marx, N. *"Cardiovascular Disease in Chronic Kidney Disease".* **Circulation** 143, 1157–1172 (2021).
8. Jdiaa, S. S., Mansour, R., Alayli, E.A., *et al. "COVID–19 and chronic kidney disease: an updated overview of reviews".* **J Nephrol** 35, 69–85 (2022).
9. Whaley-Connell, A., Nistala, R. & Chaudhary, K. *"The importance of early identification of chronic kidney disease".* **Mo Med** 108, 25–8 (2011).

10. Chen, T. K., Knicely, D. H. & Grams, M. E. *"Chronic Kidney Disease Diagnosis and Management".* **JAMA** 322, 1294 (2019).

11. Stevens, P. E., Levin, A. *et al. "Kidney Disease: Improving Global Outcomes Chronic Kidney Disease Guideline Development Work Group Members. Evaluation and management of chronic kidney disease: synopsis of the kidney disease: improving global outcomes 2012 clinical practice guideline".* **Ann Intern Med** 158, 825–30 (2013).

12. Perazella, M. A. *"The Urine Sediment as a Biomarker of Kidney Disease".* **American Journal of Kidney Diseases** 66, 748–755 (2015).

13. Canki, E., Kho, E. & Hoenderop, J. G. J. *"Urinary biomarkers in kidney disease".* **Clinica Chimica Acta.** 555, 117798 (2024).

14. Pandhi, P. Streng, K.W., Anker, S.D., *et al. "The value of spot urinary creatinine as a marker of muscle wasting in patients with new-onset or worsening heart failure".* **J Cachexia Sarcopenia Muscle** 12, 555–567 (2021).

15. Wyss,M., Kaddurah-Daouk R. *"Creatine and creatinine metabolism".* **Physiol Rev** 80(3), 1107-1213 (2000).

16. Liu, K.Z., Tian, G., Ko, A.C., *et al. "Detection of renal biomarkers in chronic kidney disease using microfluidics: progress, challenges and opportunities".* **Biomed Microdevices** 22, 29 (2020).

17. Lei, R., Huo, R. & Mohan, C. *"Current and emerging trends in point-of-care urinalysis tests".* **Expert Rev Mol Diagn** 20, 69–84 (2020).

18. Drain, P. K., Hyle, E.P., Noubary, F., *et al. "Diagnostic point-of-care tests in resource-limited settings".* **Lancet Infect Dis** 14, 239–249 (2014).

19. Naseri, M., Ziora, Z. M., Simon, G. P. & Batchelor, W. *"ASSURED-compliant point-of-care diagnostics for the detection of human viral infections".* **Rev Med Virol** 32, (2022).

20. Wu, J., Tomsa, D., Zhang, M., Komenda, P., Tangri, N., Rigatto, C., Lin, F. *"A Passive Mixing Microfluidic Urinary Albumin Chip for Chronic Kidney Disease Assessment".* **ACS Sens** 3, 2191–2197 (2018).

21. Husdan, H. & Rapoport, A. *"Estimation of creatinine by the Jaffe reaction. A comparison of three methods".* **Clin Chem** 14, 222–38 (1968).

22. Toora, B. D. & Rajagopal, G. *"Measurement of creatinine by Jaffe's reaction--determination of concentration of sodium hydroxide required for maximum color development in standard, urine and protein free filtrate of serum".* **Indian J Exp Biol** 40, 352–4 (2002).

23. Choi, S., Lee, M. G. & Park, J.-K. *"Microfluidic parallel circuit for measurement of hydraulic resistance".* **Biomicrofluidics** 4, 034110 (2010).

24. Beebe, D. J., Mensing, G. A. & Walker, G. M. *"Physics and Applications of Microfluidics in Biology".* **Annu Rev Biomed Eng** 4, 261–286 (2002).

25. Jeon, N. L. *"Generation of Solution and Surface Gradients Using Microfluidic Systems".* **Langmuir** 16, 8311–8316 (2000).

26. Debus, B., Kirsanov, D., Yaroshenko, I., *et al. "Two low-cost digital camera-based platforms for quantitative creatinine analysis in urine".* **Anal Chim Acta** 895, 71–79 (2015).

27. Tong, X., Ga, L., Zhao, R. & Ai, J. *"Research progress on the applications of paper chips".* **RSC Adv** 11, 8793–8820 (2021).

28. Dong, M., Wu, J., Ma, Z., *et al. "Rapid and Low-Cost CRP Measurement by Integrating a Paper-Based Microfluidic Immunoassay with Smartphone (CRP-Chip)".* **Sensors** 17, 684 (2017).

29. Tang, M., Wang, G., Kong, S.K. & Ho, H.P. *"A Review of Biomedical Centrifugal Microfluidic Platforms".* **Micromachines (Basel)** 7, 26 (2016).

30. Olivier, F., Maurice, A. A., Meyer, D. & Gabriel, J.C. P. *"Liquid–liquid extraction: thermodynamics–kinetics driven processes explored by microfluidics".* **Comptes Rendus. Chimie** 25, 137–148 (2022).

31. Dewandre, A., Rivero-Rodriguez, J., Vitry, Y., Sobac, B. & Scheid, B. *"Microfluidic droplet generation based on non-embedded co-flow-focusing using 3D printed nozzle".* **Sci Rep** 10, 21616 (2020).

32. Cao, J., Russo, D. A., Xie, T., Groß, G. A. & Zedler, J. A. Z. *"A droplet-based microfluidic platform enables high-throughput combinatorial optimization of cyanobacterial cultivation".* **Sci Rep** 12, 15536 (2022).

33. Glasgow, I. & Aubry, N. *"Enhancement of microfluidic mixing using time pulsing".* **Lab Chip** 3, 114–120 (2003).

34. Nielsen, J. B., Hanson, R.L., Almughamsi, H.M., *et al. "Microfluidics: Innovations in Materials and Their Fabrication and Functionalization".* **Anal Chem** 92, 150–168 (2020).

35. Gopinathan, K. A., Mishra, A., Mutlu, B. R., Edd, J. F. & Toner, M. *"A microfluidic transistor for automatic control of liquids".* **Nature** 622, 735–741 (2023).

36. Zhao, B., Cui, X., Ren, W., *et al. "A Controllable and Integrated Pump-enabled Microfluidic Chip and Its Application in Droplets Generating".* **Sci Rep** 7, 11319 (2017).

37. Liu, J. F., Yadavali, S., Tsourkas, A. & Issadore, D. *"Microfluidic diafiltration-on-chip using an integrated magnetic peristaltic micropump".* **Lab Chip** 17, 3796–3803 (2017).

38. Yen, P.W., Lin, S.C., Huang, Y.C., *et al. "A Low-Power CMOS Microfluidic Pump Based on Travelling-Wave Electroosmosis for Diluted Serum Pumping".* **Sci Rep** 9, 14794 (2019).

39. von der Ecken, S., Sklavounos, A. A. & Wheeler, A. R. *"Vertical Addressing of 1-Plane Electrodes for Digital Microfluidics".* **Adv Mater Technol** 7, (2022).

40. Mosadegh, B., Kuo, C.H., Tung, Y.C., *et al. "Integrated elastomeric components for autonomous regulation of sequential and oscillatory flow switching in microfluidic devices".* **Nat Phys** 6, 433–437 (2010).

41. Yafia, M., Ymbern, O., Olanrewaju, A.O., *et al. "Microfluidic chain reaction of structurally programmed capillary flow events".* **Nature** 605, 464–469 (2022).

42. Temiz, Y. & Delamarche, E. *"Sub-nanoliter, real-time flow monitoring in microfluidic chips using a portable device and smartphone".* **Sci Rep** 8, 10603 (2018).

43. Schuster, B., Junkin, M., Kashaf, S.S., *et al. "Automated microfluidic platform for dynamic and combinatorial drug screening of tumor organoids".* **Nat Commun** 11, 5271 (2020).

44. Gonzalez-Suarez, A. M., Long, A., Huang, X. & Revzin, A. *"A Compact Control System to Enable Automated Operation of Microfluidic Bioanalytical Assays"*. **Biosensors (Basel)** 12, 1160 (2022).

45. Watson, C. & Senyo, S. *"All-in-one automated microfluidics control system"*. **HardwareX** 5, e00063 (2019).

46. Choi, J., Kang, D., Han, S., Kim, S. B. & Rogers, J. A. *"Thin, Soft, Skin-Mounted Microfluidic Networks with Capillary Bursting Valves for Chrono-Sampling of Sweat"*. **Adv Healthc Mater** 6, (2017).

47. Narayanamurthy, V., Jeroish, Z.E., Bhuvaneshwari, K.S., *et al. "Advances in passively driven microfluidics and lab-on-chip devices: a comprehensive literature review and patent analysis"*. **RSC Adv** 10, 11652–11680 (2020).

48. Lin, P.H. & Li, B.R. *"Passively driven microfluidic device with simple operation in the development of nanolitre droplet assay in nucleic acid detection"*. **Sci Rep** 11, 21019 (2021).

49. Behera, P. P., Mohammadi, S., Li, X. *et al. "Integrated microfluidic devices for point-of-care detection of bio-analytes and disease"*. **Sensors & Diagnostics** 2, 1437–1459 (2023).

50. Narayanamurthy, V., Jeroish, Z.E., Bhuvaneshwari, K.S., *et al. "Advances in passively driven microfluidics and lab-on-chip devices: a comprehensive literature review and patent analysis"*. **RSC Adv** 10, 11652–11680 (2020).

51. Webster, A. C., Nagler, E. V, Morton, R. L. & Masson, P. *"Chronic Kidney Disease"*. **The Lancet** 389, 1238–1252 (2017).

52. GBD 2017 Risk Factor Collaborators, Stanaway, J. D. *et al. "Global, regional, and national comparative risk assessment of 84 behavioural, environmental and occupational, and metabolic risks or clusters of risks for 195 countries and territories, 1990–2017: a systematic analysis for the Global Burden of Disease Study 2017".* **The Lancet** 392, 1923–1994 (2018).

53. Disch, A., Mueller, C. & Reinecke, H. *"Low cost production of disposable microfluidics by blister packaging technology".* **Annu Int Conf IEEE Eng Med Biol Soc** 2007, 6323–6 (2007).

54. Smith, S., Sewart, R., Becker, H., Roux, P. & Land, K. *"Blister pouches for effective reagent storage on microfluidic chips for blood cell counting".* **Microfluid Nanofluidics** 20, 163 (2016).

55. *"National Kidney Foundation. K/DOQI clinical practice guidelines for chronic kidney disease: evaluation, classification, and stratification".* **Am J Kidney Dis** 39, S1-266 (2002).

56. Warner-Tuhy, Alana. *"Mass transfer of urea, creatinine and vitamin B-12 in a microchannel based membrane separation unit".* **Graduate Thesis. Oregon State University** (2009).

57. Orabona, E., Caliò, A., Rendina, I., Stefano, L. & Medugno, M. *"Photomasks Fabrication Based on Optical Reduction for Microfluidic Applications".* **Micromachines (Basel)** 4, 206–214 (2013).

58. Johnsona, D. W., G. J., S. V., & Y. D. *"SUEX Dry Film Resist – A new Material for High Aspect Ratio Lithography".* (2012).

59. Sahin, O., Ashokkumar, M. & Ajayan, P. M. *"Micro- and nanopatterning of biomaterial surfaces".* in **Fundamental Biomaterials: Metals** 67–78 (Elsevier, 2018).

60. IUPAC. Compendium of Chemical Terminology, 2nd ed. (the "Gold Book"). Compiled by A. D. McNaught and A. Wilkinson. Blackwell Scientific Publications, Oxford (1997).

Chapter 3: Integrated microfluidic immunoassays for point-of-care diagnostic measurement of human serum Cystatin C in chronic kidney disease

This chapter is based on part of the following publication: "Tomsa, D., Liu, Y., Abolfathi, A.H., Lin, F. *et al. "Integrated microfluidic immunoassays for point-of-care diagnostic measurement of human serum Cystatin C in chronic kidney disease".* (**Submitted for journal publication. Under review.**)"

In this project, we developed a PDMS-based microfluidic immunoturbidity chip allowing side-scattering optical measurement. We demonstrated that the chip meets detection limit and range requirements for clinical CYS-C measurement. In validation studies using serum samples from CKD patients across different CKD stages, chip tests showed a similar agreement level with the traditional well plate-based immunoturbidity assay test results.

In this study, I assembled the system, designed and fabricated the CYS-C PDMS turbidity assay chip, conducted the experiments, analyzed the data, and wrote the manuscript.

3.1 Abstract

CYS-C is considered a superior to creatinine as a serum biomarker of eGFR. It is minimally influenced by non-filtration-specific factors such as muscle mass, age, and gender. However, currently CYS-C testing is limited to specialized diagnostic labs, and no PoC tools are clinically available. To address this gap, we leveraged the enabling power of microfluidic devices for PoC tests of CYS-C. In this study, we developed a PDMS-based microfluidic immunoturbidity chip allowing side-scattering optical measurement for quantitative CYS-C tests. We demonstrated that the chip meets the clinical requirements of the serum CYS-C detection range and limit. Importantly, the microfluidic chip is integrated with a custom-developed portable reader as PoC test prototypes. In validation studies using serum samples from CKD patients across different disease stages, chip tests showed a similar agreement level with the traditional well plate-based immunoturbidity assay test results. The microfluidic assay offers practical solutions for decentralized PoC diagnostic tests of CKD with competitive advantages over existing methods.

3.2 Introduction

CKD diagnosis typically involves eGFR, often calculated from serum creatinine. While serum creatinine is widely used, it is influenced by factors such as age, sex, race, muscle mass, and nutrition, limiting its accuracy[1,2]. In contrast, serum CYS-C offers a more reliable biomarker for GFR estimation. Produced by all nucleated cells, CYS-C levels are stable and less affected by non-renal factors[3–6]. Notably, CYS-C has been shown to predict long-term mortality better than creatinine in critically ill patients[7]. Beyond nephrology, CYS-C has been implicated in cardiovascular disease progression and neurodegenerative disorders such as Alzheimer's disease[8–12].

Despite its clinical value, CYS-C testing remains largely restricted to laboratory settings due to the complexity, cost, and infrastructure required for current methods. Techniques such as ELISA, radioimmunoassays, immunoturbidimetry, fluorescence-based assays, and mass spectrometry are accurate but demand skilled personnel, expensive reagents, and time-intensive workflows[13–15]. These limitations hinder the widespread adoption of CYS-C testing, especially in primary care or low-resource environments.

To address this gap, a true PoC test for CYS-C must balance simplicity, cost-effectiveness, speed, and analytical accuracy. Microfluidic technologies offer a promising foundation for such solutions. By miniaturizing lab processes onto portable chips, microfluidic PoC devices can deliver rapid, user-friendly, and reliable diagnostics[16–18]. Most existing CYS-C microfluidic devices rely on electrochemical sensing, using complex electrode materials—such as ZIF-8-Cu1−xNix(OH)2@Cu[19], graphene composites[20], and MOF-based nanomaterials[21] to enhance performance. While sensitive, these designs are often prohibitively difficult to mass-produce. Turbidimetric and nephelometric detection

strategies are more suited to scalable and low-cost implementation but remain underexplored in this context. A continuous-flow microfluidic turbidity sensor was previously developed for non-diagnostic use[22], and a latex immunoagglutination assay for vasculitis marker detection inspired our current direction[23].

In this study, we present a microfluidics-based approach for PoC quantification of serum CYS-C. A PDMS-based turbidimetric immunoassay, leveraging the particle-enhanced turbidimetric immunoassay (PETIA) principle. PETIA provides a fast, sensitive, and specific quantification of antigen-antibody complexes[15,24–26], and PDMS platforms enhance assay control, portability, and throughput. Our device is built on this foundation, introducing innovations to enable quantitative CYS-C detection in a cost-effective, accessible format.

3.3 Results

3.3.1 PDMS-based microfluidic immunoturbidity chip for Cystatin C measurement

The PDMS-based microfluidic immunoturbidity chip is designed to allow side-scattering light measurement of the analyte in the continuous passive flow. An optical probe at the direction of the scattered light from the OW can measure the side-scattering light intensity and thus quantitatively correlate it to the CYS-C concentration in the sample. Each test unit on the microfluidic chip has 4 connected functional elements (**Fig. 3.1a**), including **1)** an inlet well, which is used for loading the working solution containing a mixture of reacted CYS-C sample in the buffer (R1) with antibody-coated microparticles (R2); **2)** an OW that has a lenticular shape and can fit a 2 mm diameter circle in its widest part. The size of the OW was chosen to ensure the ease of alignment with the light source, and the lenticular shape of the OW was adapted from our previously developed urine creatinine test chip, which helps reduce flow speed variation within the OW[27]; **3)** a hydraulic resistor connecting the

OW and the outlet to reduce and stabilize the flow over 20 minutes, which provides enough assay time window for multiple measurements if needed; and finally; **4)** an outlet well for waste collection, which is initially emptied to ensure a sufficient negative pressure gradient relative to the inlet well during the test.

The chip pattern was fabricated using 100 μm thick dry-film photoresist on a 3-inch silicon wafer (**Fig. 3.1b**). Besides being a cleaner and simpler photolithography fabrication process compared with liquid SU-8 photoresist, the dry-film photoresist produces a more uniform pattern thickness[27,28]. Using this fabrication method, we configured 10 microfluidic test units on a single master mold. The size, dimensions, and layout of the pattern were designed so that the PDMS replica from the master mold can fit the 10 test units on a single 50 x 75 mm glass slide for a higher throughput experiment (**Fig. 3.1c**). PDMS was chosen as the final chip material for its excellent optical transparency to enable turbidity measurement with low background noise from the chip material itself.

At first, direct optical imaging was considered a straightforward turbidity detection method. As expected, phase contrast images of the reacted CYS-C turbidity solution in the OW of the microfluidic chip clearly show larger particle aggregates over increasing CYS-C concentrations (**Fig. 3.1d**), confirming effective CYS-C immunoturbidity chemistry. However, the imaging approach is insufficient to quantitatively measure different CYS-C concentrations. Therefore, a more accurate optical detection method was required. In this direction, we next configured a microscope setup with the high-power, focused, and wavelength-filtered light beam as well as a spectrometer to allow side-scattering light measurement from the CYS-C turbidity solution in the OW of the microfluidic chip (**Fig. 3.S1a**). Consistent with the data provided by the manufacturer of the turbidity reagent kit

using the traditional static reaction chamber, the recommended 3:1 (R1:R2) mixing ratio resulted in a non-linear calibration curve and signal saturation after 4 mg/L in our turbidity chip test (**Fig. 3.S1b**). Because of the flow-based side-scattering signal detection in our turbidity chip, we explored the possibility of improving the linear detection range by optimizing the reagents' mixing ratio. Indeed, changing the ratio to 2:1 (R1:R2), which effectively enhanced the binding reaction, resulted in a linear detection range up to 8 mg/L with the R^2=0.9162 (**Fig. 3.S1c**). Furthermore, adding the initial reference signal subtraction step at the same 2:1 ratio, which calibrated the initial signal variation, achieved an even higher linearity of the calibration curve at R^2=0.9909 (**Fig. 3.S1d**).

3.3.2 Integrated Cystatin C test with the microfluidic turbidity chip and a compact nephelometer

To enable PoC tests outside specialized labs, a portable nephelometer prototype was designed as a miniaturized version of our previous large microscope setup (**Fig. 3.2A**). The CYC-C concentration-dependent microparticle aggregates interfere with the incident light by redirecting and scattering it further away from the incident direction. In our setup (**Fig. 3.2B**), the optic fiber probe is fixed at 45° to the stage plane, which is within the angle range for scattered light measurements from 30° to 90° degrees[29] but avoid the extreme angles, which can cause more noise due to reflection and scattering of light from the 3D-printed frames. The blue LED with a heat sink was placed inside an adjustable frame above the platform stage as the incident light source. The nephelometer frame was printed from black ABS filament to reduce the amount of stray light captured by the probe. The results obtained from each test were saved as a series of light spectrums. The materials used to build the portable nephelometer and the reagents involved in the immunoturbidity assay are not

fluorescent; therefore, the probe can faithfully measure the scattered light intensity without spectrum changes. Based on this consideration, the scattered light intensity can be simply obtained by measuring the peak value of the spectrum or, alternatively, by measuring the full spectrum. For the latter approach, we integrated the light intensity measurement over the full width half maximum (FWHM) and then normalized it to the maximum as the final scattered light intensity for subsequent analysis. Using a single end-point scattered light measurement to mimic the practical PoC test, our integrated CYS-C test with the microfluidic turbidity chip and the compact nephelometer clearly demonstrated the uplifted scattered light spectrum with increased CYS-C concentrations as expected (**Fig. 3.3A**). Quantitatively, it achieved an impressive LOD of 0.07 mg/L (**Fig. 3.3B**), significantly below the clinical threshold between normal and CKD, and an upper detection limit of at least 4 mg/L, which exceeds the clinical cut-off level between moderate and more advanced stages of CKD. On the other hand, the current test protocol, although it meets the PoC test requirements in terms of ease of operation and rapid test result reporting, yields a non-linear calibration curve, which motivated further optimization to improve prediction accuracy.

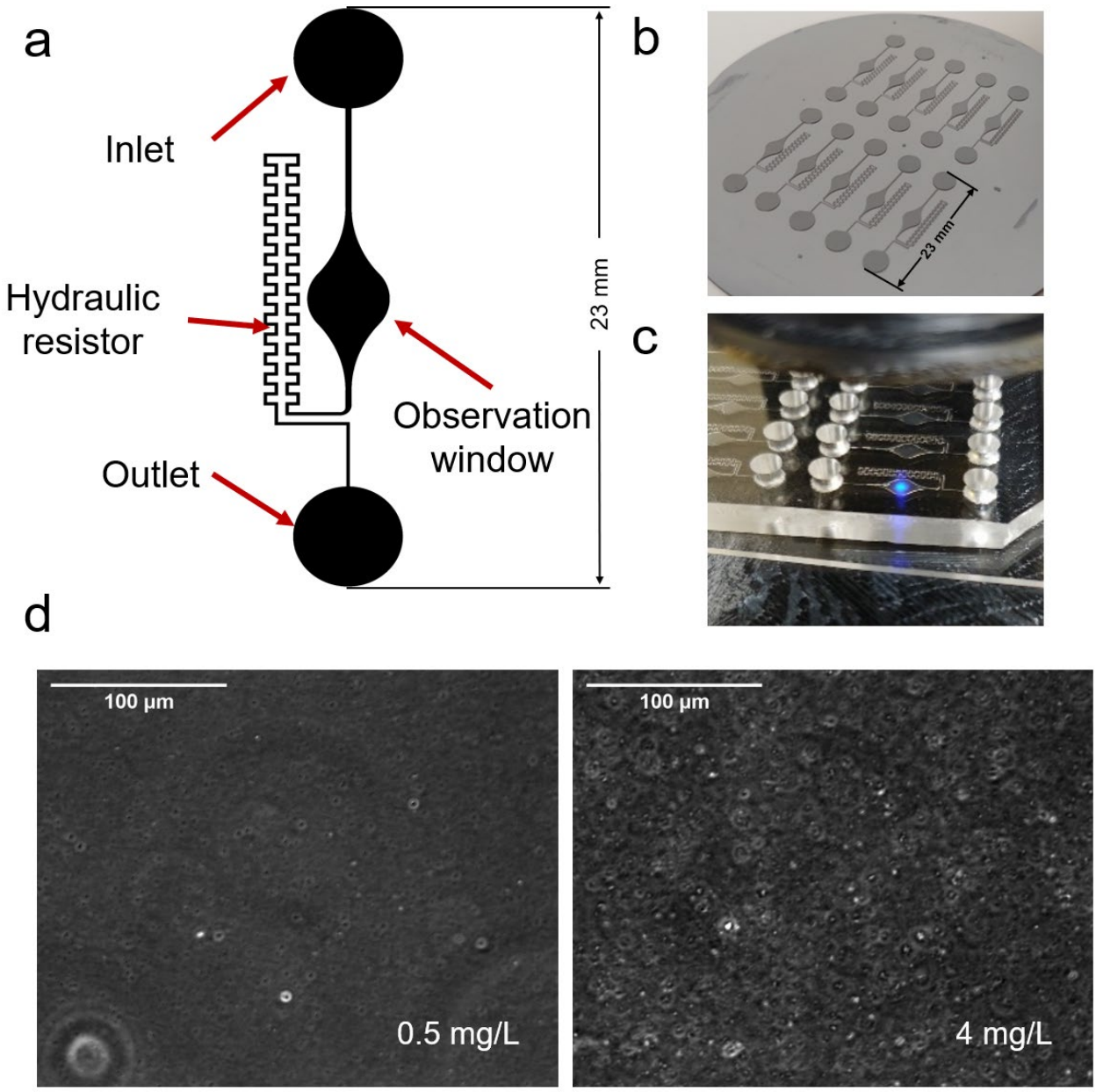

Figure 3.1 Illustration of the CYS-C turbidity immunoassay chip.

a. The CYS-C turbidimetric chip design is illustrated. The observation window diameter is 2 mm and the hydraulic resistor is ~60 mm long with a channel cross section of 100 µm x 100 µm; **b.** A picture of the master mold used for making PDMS microfluidic chips is shown; **c.** A picture of the PDMS-based microfluidic chip measured by the microscope-based nephelometer is shown. The blue LED light (~1 mm in diameter) incidents on the observation window in one of the test units; **d.** Phase contrast images (40X magnification) show the larger microparticle aggregates in the CYS-C standard of 4 mg/L compared to it in the CYS-C standard of 0.5 mg/L on the microfluidic chip.

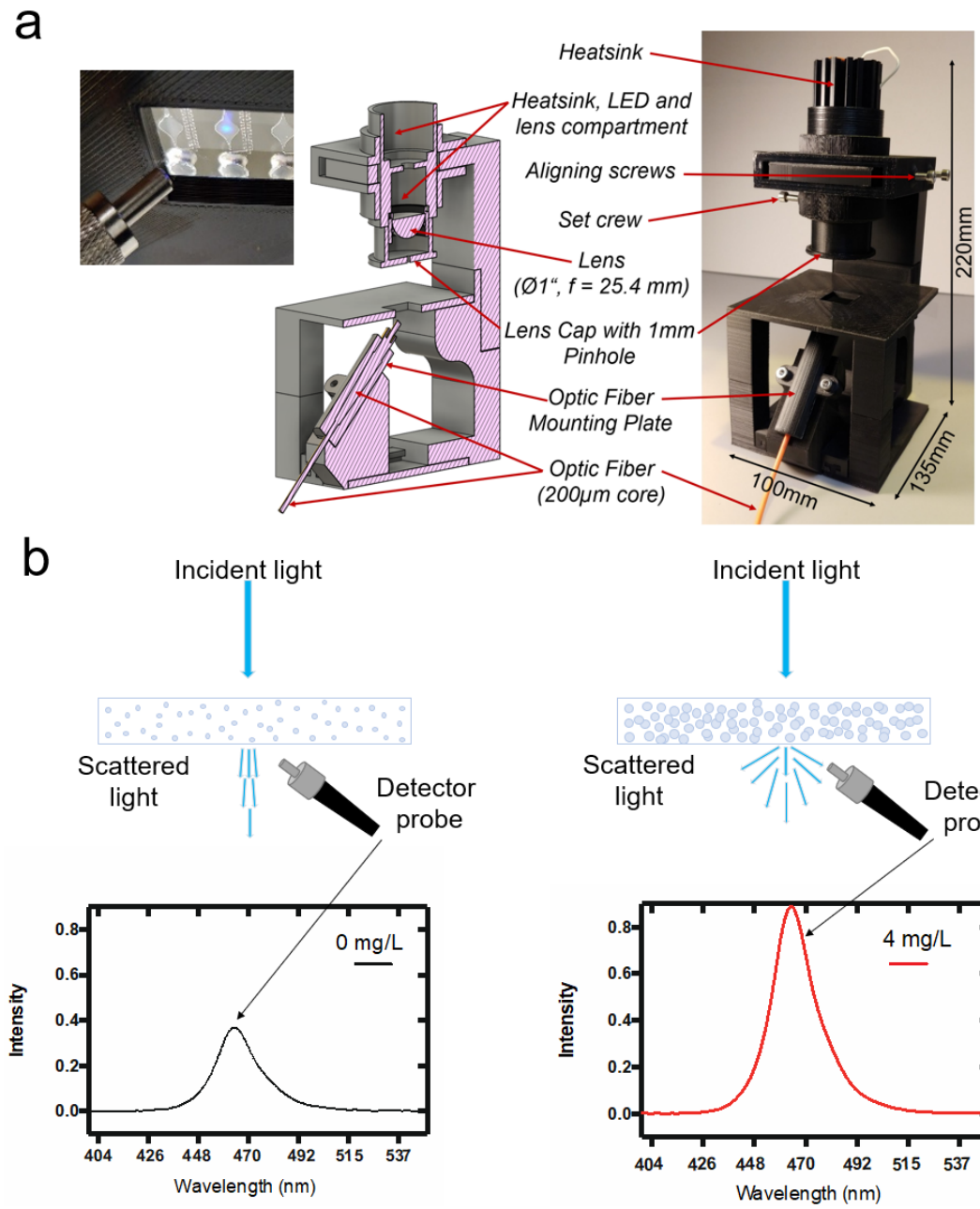

Figure 3.2 Compact nephelometer for the turbidity immunoassay chip

a. The compact nephelometer setup for turbidity immunoassay chip measurements is illustrated. The frame was 3D printed from black plastic to reduce light reflections and background noise. The light source is composed of a blue LED and lens, and the aperture/pinhole is used to "trim" the light beam to ~1 mm diameter. The optic fiber probe is placed at 45˚ under the stage and ~10 mm from the observation window; **b.** The schematic representation of the nephelometer working principle and the representative scattered light spectrum are presented comparing 4 mg/L of CYS-C standard and the blank. The intensity of the scattered light is correlated to concentration and size of the dissolved or suspended particles in the sample solutions.

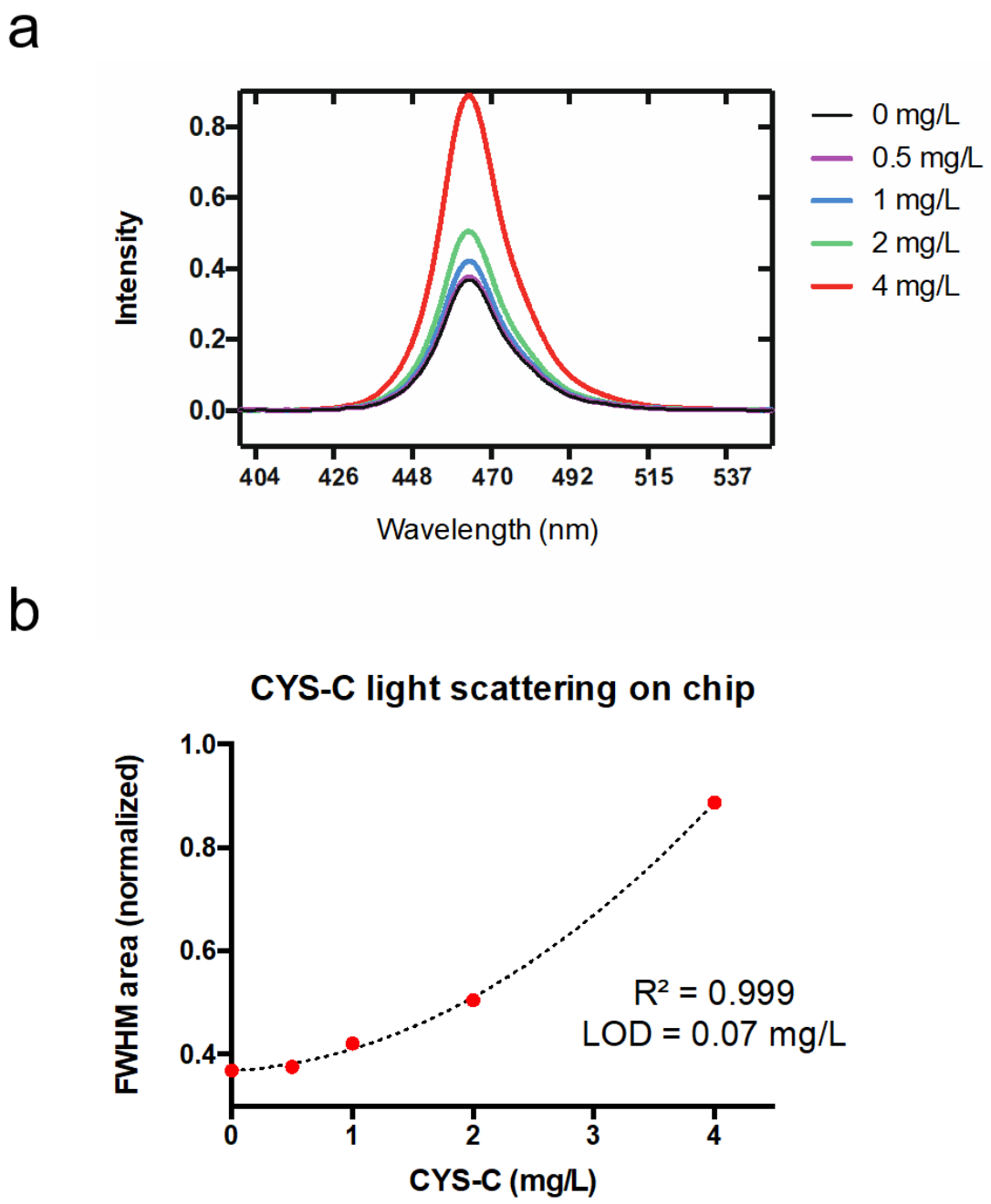

Figure 3.3 Technical characterizations of the turbidity immunoassay chip with the compact nephelometer

a. The spectra of the scattered light for different CYS-C concentrations ranging from 0 to 4 mg/L are shown; **b.** The calibration curve based on the normalized FWHM area of the spectrum against the CYS-C standard concentrations from (**a**) is shown.

3.3.3 Clinical sample validation of the microfluidic Cystatin C immunoassays for diagnostic test of chronic kidney disease

Based on satisfactory technical calibration of the developed CYS-C turbidity chip test method, we performed further validation studies using serum samples from patients who have been diagnosed with CKD. The collected patient data included age, gender, serum CRE (μmol/L), eGFRcr value (eGFR based on the clinically measured serum creatinine level, mL/min/1.73 m²), uACR (mg/mmol), and CKD stage (**Table 3.1**). The CKD stages were classified based on the eGFRcr values according to the National Collaborating Centre for Chronic Conditions (2008). CKD stages were further grouped into three categories: mild, moderate, and serious kidney function loss. Specifically, the mild kidney damage corresponds to eGFRcr values above 60 mL/min/1.73 m² (G1 and G2); the moderate kidney damage includes stages G3a and G3b, with eGFRcr values between 30 and 59 mL/min/1.73 m²; and the severe kidney damage (stages G4 and G5) is defined by eGFRcr values below 30 mL/min/1.73 m². A total of 24 CKD samples covering these three CKD groups with the eGFRcr range spanning from 18 to 146 mL/min/1.73 m² were tested for chip validations.

The general trend of the inverse proportionality between the filtration markers (i.e., clinically determined serum creatinine or chip-measured serum CYS-C) and their respective eGFR based on the filtration marker-specific estimation formula was first verified in these clinical CKD samples (**Fig. 3.S3**). Next, as a primary technical validation measure, we quantitatively compared the chip test results of CYS-C for these 24 CKD serum samples to a reference test method (turbidimetric well test). Instead of the conventional linear regression-based correlation analysis, we applied the well-established and considerably more effective Bland-Altman (B-A) analysis[30] to assess the system bias between the chip

measurements and the reference immunoturbidity assay in the standard well-plate format. In the B-A analysis, the difference between the two methods was plotted against the average of the two measurements. Our results showed that for the turbidity chip test, the mean difference is slightly more than 1 mg/L (i.e., 1.219 mg/L for the turbidity chip and 1.274 mg/L for the paper chip), and most of the test data falls within the limit of agreement (LoA), which is calculated as the 95% confidence intervals (i.e., +/- 1.96 times the standard deviation of the mean difference) (**Fig. 3.4**). In the context of CKD, serum CYS-C levels above 0.95 mg/L typically indicate impaired kidney function, while levels below 0.95 mg/L are generally considered within the normal range[31]. A survey of 141 laboratories reported mean CYS-C values for CKD samples ranging from 2.052 to 2.909, highlighting significant variability and high biases across different lab tests[32,33]. Therefore, given the mean bias and the data spread around the mean bias according to the B-A analysis, we next designed our secondary analysis to evaluate the CKD stage prediction accuracy based on the chip test and the CKD-EPI CYS-C Equation for eGFR against the clinical eGFRcr values as the comparison reference.

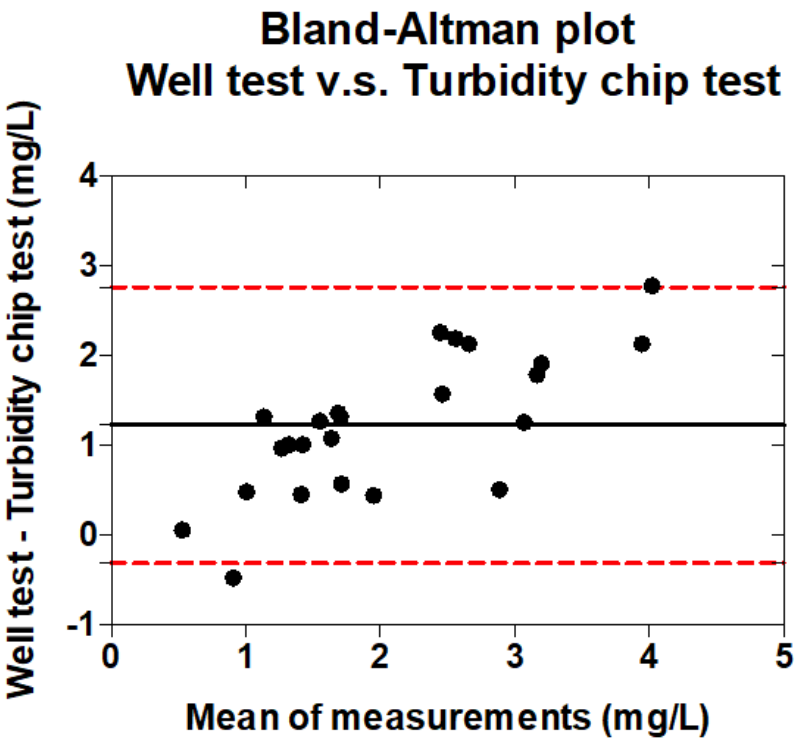

Figure 3.4 Bland-Altman (B-A) Analysis comparing the CYS-C chip test with the reference test using the well-plate turbidity assay of the 24 clinical CKD samples

The B-A plot compares the CYS-C turbidity test with the reference test using the well-plate turbidity assay. The black solid line is the mean difference between the chip test and the reference test (well-plate test – chip test); The red dashed lines are the limit-of-agreement range (LoA) calculated as ±1.96 x mean difference;

ID	Age	Gender	serum CRE (μmol/L)	eGFR (mL/min/1.73m^2)	CDK stage	uACR (mg/mmol)
1	37	F	43.3	124	1 or 2	1.3
2	73	F	49.8	96	1 or 2	2.2
3	56	M	51.3	114	1 or 2	7
4	21	F	33.7	146	1 or 2	3.4
5	71	F	58.9	94	1 or 2	4
6	52	M	85.2	95	1 or 2	0.7
7	52	M	75.2	105	1 or 2	3.6
8	59	F	78.3	75	1 or 2	7.5
9	49	M	70.8	108	1 or 2	26
10	60	M	83	93	1 or 2	22.4
11	67	M	106.5	66	1 or 2	0.9
12	71	F	117.2	43	3a	8.3
13	74	M	124	53	3a	4.2
14	78	F	105	47	3b	22.9
15	74	F	100.7	51	3a	36.2
16	76	M	162.4	38	3b	0.4
17	59	M	188.4	35	3b	7
18	72	M	207.1	29	4	3.2
19	72	M	160.4	39	3b	28.9
20	35	M	180.4	43	3b	30.1
21	88	M	253.3	20	4	10.7
22	56	M	247.2	26	4	16.6
23	72	M	291.2	19	4	31
24	73	F	237	18	4	128.9

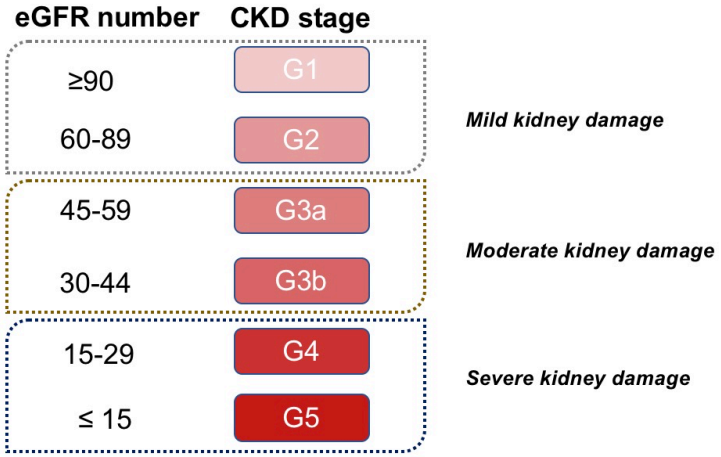

Table 3.1 CKD patients clinical information summary.

Top. The 24 CKD patients' serum creatinine (μmol/L), eGFRcr (mL/mim/1.73m2), age, gender, and uACR values are shown; **Bottom.** CKD stage and kidney damage classification based on eGFRcr are shown (generated in reference to the National Collaborating Centre for Chronic Conditions (2008)).

Proceeding with the CKD stage prediction accuracy analysis, we first applied a simple binary approach to evaluate the eGFR prediction accuracy based on our CYS-C chip tests (eGFRcys-c) against the clinically determined eGFRcr values as the hypothetical ground truth. Clinically, an eGFRcr of 90 mL/min/1.73 m^2 or higher is considered normal; an eGFRcr below 60 mL/min/1.73 m^2 indicates kidney disease; and an eGFRcr below 15 mL/min/1.73 m^2 signifies kidney failure. Thus, we analyzed the diagnostic accuracy of our CYS-C chip test to distinguish between normal and CKD using the cutoff eGFRcr 60 mL/min/1.73 m^2. **Table 3.2** summarizes the binary-based prediction accuracy evaluators, including sensitivity, specificity, positive predictive value (PPV), negative predictive value (NPV), and overall accuracy. Among the 24 clinical samples, 20 samples were correctly predicted using the CYS-C turbidity chip (accuracy: 83%). These results motivated us to further evaluate the prediction accuracy at higher resolution. Specifically, we analyzed the prediction accuracy of the chip test based on the three CKD stage categories as defined in **Table 3.1**. Our results showed that the turbidity chip test achieved relatively high accuracy (> 80%) in classifying patients with eGFRcr > 60 or < 30 mL/min/1.73 m^2 for the mild or severe stage, respectively, whereas the prediction accuracy for the moderate CKD stage (eGFRcr 30–59 mL/min/1.73 m^2) is lower (< 80%), as expected (**Table 3.S1**).

Two-Stage Diagnostic Accuracy of the CYS-C Chip Test (based on eGFR<60)

		Clinical eGFR (serum CRE)		
		Positive	Negative	Total
CYS-C Turbidity chip	Positive	11	2	13
	Negative	2	9	11
	Total	13	11	24

	Sensitivity	Specificity	PPV	NPV	Accuracy
CYS-C Turbidity chip	85%	82%	85%	82%	83%

Table 3.2 Two-stage (binary-based) eGFR diagnosis accuracy based on the CYS-C chip test using the 24 clinical CKD samples

Top. Cross-tabulation table comparing the CYS-C chip predicted eGFRcys-c against the clinical creatinine predicted eGFRcr is shown; **Bottom.** The accuracy evaluators based on data in the **Top** table including the sensitivity, specificity, PPV, NPV, and overall accuracy, are shown.

	ELISA	Turbidity assay	CYS-C turbidity chip
Detection	colorimetric	turbidity	spectrometry
Reaction	sandwich immunoassay	immunoturbidimetry	immunoturbidimetry
Sample volume	100 µL	1.5 µL	1.5 µL
LOD	10 pg/mL	0.3 mg/L	0.07 mg/L
Detection range	0.312~20 ng/mL	0.5~8.0 mg/L	0.5~4.0 mg/L
Assay duration	4.5 hrs	~20 mins	~20 mins
Cost (CAD)	~$20 / sample	~$20 / sample	~ $2.1 / test
User skills level	high	high	medium
Portable reader	no	no	yes
Suitable for PoC	no	no	yes

Table 3.3 Comparison of the CYS-C turbidity chip with selected commercial CYS-C test

3.4 Discussion

In this study, we developed a microfluidic solution for PoC measurement of serum CYS-C as an important diagnostic biomarker for CKD. In our current integrated CYS-C turbidity chip test with the portable nephelometer, we achieved a calibration curve covering the full clinically relevant range and the satisfactory detection limit (**Fig. 3.3B**). However, this calibration curve was best fitted with a nonlinear function. Compared to the large microscope setup, the portable nephelometer used a low-power light source and inexpensive optical parts to keep the cost lower. In addition, compared to the microscope-based test protocol, the portable test adapted the standard 3:1 (R1:R2) reagent mixing ratio without initial reference signal subtraction to allow simpler and faster tests for PoC applications. We believe these factors contributed to the nonlinear calibration curve. To enable the preferable linear calibration curve on the portable nephelometer part, we propose to upgrade it by using a higher intensity light source, such as a laser, or combining high-intensity LEDs with proper optics for improved light focusing. In the test protocol part, we will use the optimized 2:1 (R1:R2) reagent mixing ratio for the test as well as the automated reference initial signal measurement to allow kinetic signal calibration. Altogether, these proposed modifications are expected to improve the technical performance of the CYS-C turbidity test. Importantly, our immunoturbidity chip platform is not limited to CYS-C measurement but can be readily adapted to other health biomarkers. One such example is urine albumin, another key CKD diagnostic biomarker, and the immunoturbidity assay is the current standard test method[34], which therefore can be readily adapted into the turbidity chip to allow potential integrated multi-marker tests for CKD screening and diagnosis on a single microfluidic immunoturbidity test platform.

Previous studies have demonstrated the superior performance of CYS-C-based eGFR determination in specific patient populations[35]. For instance, in renal transplant recipients, $eGFR_{cys-c}$ was found to be more accurate than traditional creatinine-based equations[36]. Similar findings were reported in patients with rheumatoid arthritis and secondary amyloidosis[37] and cirrhotic patients[38]. Additionally, studies have suggested that eGFR determination can be further improved by incorporating both creatinine and CYS-C values[39]. Indeed, the CKD-EPI Creatinine-Cystatin C Equation (2021), which integrates serum CYS-C levels, serum creatinine levels, age, gender, and race, led to more accurate eGFR[40]. In this context, our developed CYS-C chip test provides the PoC diagnostic tool required for improved eGFR determination in CKD and, furthermore, has the potential to enable integrated tests of the dual eGFR markers based on CYS-C and creatinine on a single microfluidic chip.

The most commonly used CYS-C assays include ELISA and immunoturbidity, with the latter also being the current standard clinical lab test[41]. Both methods require specialized lab facilities and skills. The ELISA test kit is typically over several hundred dollars in cost, while the immunoturbidity assay-based clinical test costs over $30 per test and often needs long-distance sample transport. According to a 2019 survey by the College of American Pathologists, only 7% of US clinical laboratories offered CYS-C tests[41,42] and clinical PoC CYS-C tests are currently not available. In this context, our CYS-C chip test presents clear technical and practical advantages over the existing test methods (**Table 3.3**). For the ideal sample-to-result PoC CYS-C test, on-chip serum or plasma isolation from whole blood is required. Collectively, our CYS-C chip test represents a transformative PoC solution to

realize the advantageous use of CYS-C for CKD diagnosis, risk monitoring, and therapeutic management.

3.5 Materials and Methods

3.5.1 Cystatin C turbidity chip test

The turbidity assay solution was prepared according to the manufacturer's recommendations. The 1.5 µL of CYS-C sample solution was dissolved in 150 µL of R1 buffer at the 1:100 ratio. The solution was then incubated at 37 °C for 5 min. Next, 50 µL or 75 µL of microparticle suspension of R2 solution containing antibody-coated particles based on the 3:1 or 2:1 mixing ratio (R1:R2) was added, well mixed, and left to react for 8 min, all in a 0.65 mL Eppendorf tube. The ~50 µL of the reacted solution was then loaded into a freshly prepared PDMS chip unit. Once all the solutions were transferred to the microfluidic chip, each unit's OW was positioned under the nephelometer's light source beam. The spectrometer was set to a 10-second integration time and an average of 3 measurements for a smooth intensity signal profile. The peak value of each signal profile was then plotted to generate the calibration curve or fit a sample's signal value to a pre-generated calibration curve to estimate the concentration. For convenience, all the intensity values were normalized to the maximum concentration of 8 µg/mL.

3.5.2 Well plate-based Cystatin C turbidity assay

The 1.5 µL of CYS-C sample solution was added to 150 µL of R1 buffer in a 96-well plate. The mixture was then incubated at 37°C for 5 min. Next, 50 µL of microparticle suspension R2 was added to each sample well, mixed, and left to react for 8 minutes. Finally, the well plate was loaded into the plate reader to obtain the turbidity values for each sample with OD 562 nm (the linear calibration curve is shown in **Fig. 3.S2**).

3.5.3 Microfluidic Cystatin C chip test with clinical serum samples from CKD patients

Serum samples from CKD patients were obtained under an approved ethics protocol by the University of Manitoba. We measured the CYS-C levels in 24 CKD serum samples using both the turbidity chip and the paper chip test. The results from the chip-based tests were further compared with the results obtained from the turbidity assay using the standard well plate format and a conventional plate reader as the reference. Detailed clinical information of the CKD patients, including age, gender, serum creatinine levels, CKD stages based on eGFR, and uACR values, is provided in **Table 3.1**.

For the CYS-C turbidity chip test, 1.5 µL of CKD serum was diluted in 150 µL of R1 buffer at the 1:100 ratio. The solution was then incubated at 37°C for 5 minutes. Subsequently, 50 µL of microparticle suspension (R2) was added to the mixture of the sample and R1 buffer, thoroughly mixed, and allowed to react for 8 minutes. Approximately 50 µL of the reacted solution was then loaded into a freshly prepared PDMS chip unit. The same batch of reaction solutions was also used for the turbidity assay in multi-well plates for comparative analysis.

3.5.4 Data analysis

For nonlinear regression, we used a second order polynomial function:

$$y = ax^2 + bx + c$$

where a, b and c are regression coefficients. The LOD was calculated by solving the quadratic equation:

$$a \times LOD^2 + b \times LOD - 3\sigma = 0$$

where σ is the standard deviation of the regression intercept.

To compare the CYS-C level in the clinical samples measured by the chip test and the reference method, we applied the standard linear regression to evaluate the correlation and, furthermore, Bland-Altman analysis, which is a the clinically accepted method to method to evaluate the equivalence between different analytical methods[43].

Based on the clinical information of the 24 CKD patients, including age, gender, and serum creatinine levels, we calculated the eGFR using the CKD-EPI Creatinine Equation (2021) as follows[16]:

$$eGFRcr = 142 \times \min\left(\frac{Scr}{\kappa}, 1\right)^{\alpha} \times \max\left(\frac{Scr}{\kappa}, 1\right)^{-1.209} \times 0.9938^{Age} \; [\times 1.012[if\ female]]$$

where: Scr = standardized serum creatinine in mg/dL; κ = 0.7 (females) or 0.9 (males); α = -0.241 (female) or -0.302 (male); min (Scr/κ, 1) is the minimum of Scr/κ or 1.0; max (Scr/κ, 1) is the maximum of Scr/κ or 1.0; Age (years).

For eGFR calculations based on CYS-C measurements, we used the CKD-EPI Cystatin C Equation (2012) as follows[1,44–46]:

$$eGFR = 133 \times \min\left(\frac{Scys}{0.8}, 1\right)^{-0.499} \times \max\left(\frac{Scys}{0.8}, 1\right)^{-1.328} \times 0.996^{Age} \; [$$
$$\times 0.932[if\ female]]$$

where: Scys = standardized serum cystatin C in mg/L; min is the minimum of Scys/0.8 or 1; max is the maximum of Scys/0.8 or 1; Age (years).

Using the eGFRcr cutoffs for CKD classification (≥60, 30–59, and <30 mL/min/1.73 m²), we categorized the 24 CKD patients into mild, moderate, and severe kidney damage groups (**Table 3.1**). We then compared the classification accuracy of eGFR predictions

derived from the CYS-C turbidity chip tests with the clinical eGFRcr formula-based predictions. The prediction accuracy metrics, including sensitivity, specificity, positive predictive value (PPV), negative predictive value (NPV), and overall accuracy, were calculated using a cross-tabulation table method[47].

Additional materials and methods are provided in the **Supplementary Information**. No unexpected or unusually high safety hazards were encountered in this study.

3.6 Supplementary Information

3.6.1 Materials

The microfluidic chip design was printed on regular paper using a Xerox ColorQube 8870 solid ink printer (Xerox, Norwalk, CT, USA). A TOYO-VIEW 4×5 camera was used to image the chip design onto the photo film. Other materials used for photomask fabrication include the photo film (Arista Ortho Litho Film 3.0-4×5), the photo developer (Arista Powder A&B Litho Developer), the photo film fixer (Ilford Rapid Fixer) and the washing solution (Kodak Photo-Flo 200). The SUEX dry film photoresist was purchased from MicroLaminates (Sudbury, MA, USA) and the 3-inch silicon wafer was ordered from Silicon Inc. (Plano, TX, USA). Dow SYLGARD™ 184 Silicone Elastomer Clear was purchased from ELLS-WORTH Adhesives (Germantown, WI, USA). The CYSTATIN-C: ITA Reagent Kit was ordered from Toronto BioScience. The LED light source focusing lens (LA1951-ML - Ø1" N-BK7 Plano-Convex Lens, SM1-Threaded Mount, f = 25.4 mm, Uncoated) and the compact spectrometer (CCS200/M) were purchased from Thorlabs. The blue LED (XPEBRY-L1-0000-00R01-SB01) was purchased from DigiKey.

3.6.2 Microfluidic Cystatin C turbidity chip design and fabrication

The chip was designed in AutoCAD (Ver. 2023). The length of the resistive channel was chosen to be ~60 mm in order to give enough duration of continuous flow. The height of the OW and resistive channel is 100 μm. The photomask was fabricated using an optical reduction technique. In short, the chip pattern was printed in black color on a standard letter-size white paper with the scale 9:1 and attached to a whiteboard for a uniform background. Then the image of the chip pattern was captured on a 4×5 film camera using the high-contrast Ortho Litho film. The film was developed following standard procedures recommended by the film manufacturer. The chip pattern was transferred to a 3-inch silicon wafer using the standard dry film photolithography method. Then the silicon wafer master mold was placed in a petri dish and filled with polydimethylsiloxane (PDMS), degassed in a desiccator for 20 min, and baked at 80°C for 1.5 hours. The cured PDMS chip replica was then carefully cast out from the mold, and 4 mm diameter holes were punched to serve as chip inlets and outlets. Next, the PDMS chip was cleaned with adhesive tape to remove any debris from the channel side. Finally, the PDMS chip was air plasma treated and bonded to a glass slide to seal the channels. The chip is typically used within ~20 min after plasma treatment before the PDMS surface recovers to the hydrophobic state.

3.6.3 Compact nephelometer for microfluidic turbidity chip

A nephelometer is an instrument that measures the intensity of the light scattered by a turbid medium, generally a liquid. The intensity of the measured signal is related to the concentration and/or size of the dissolved or suspended particles in the tested solution. The measurement is generally performed at a 30° to 90° angle and away from the direct incident light beam. The wavelength of the light source has to be considered in the case of dealing

with a fluorescent sample. Guided by this principle, the compact nephelometer design was modeled in Autodesk Fusion and 3D-printed with black plastic to reduce light reflections and background noise. The light source is composed of a blue LED, a lens with a focal length of 25.4 mm, and a pinhole to “trim” the light spot to a ~1 mm diameter. The optical fiber probe is placed at 45° under the sample stage and ~10 mm from the OW. The light source compartment is adjustable in X-Y-Z dimensions. The set screw fixes the position in the Z-axis, and the aligning screws are used to align and fix the position in the X and Y axes.

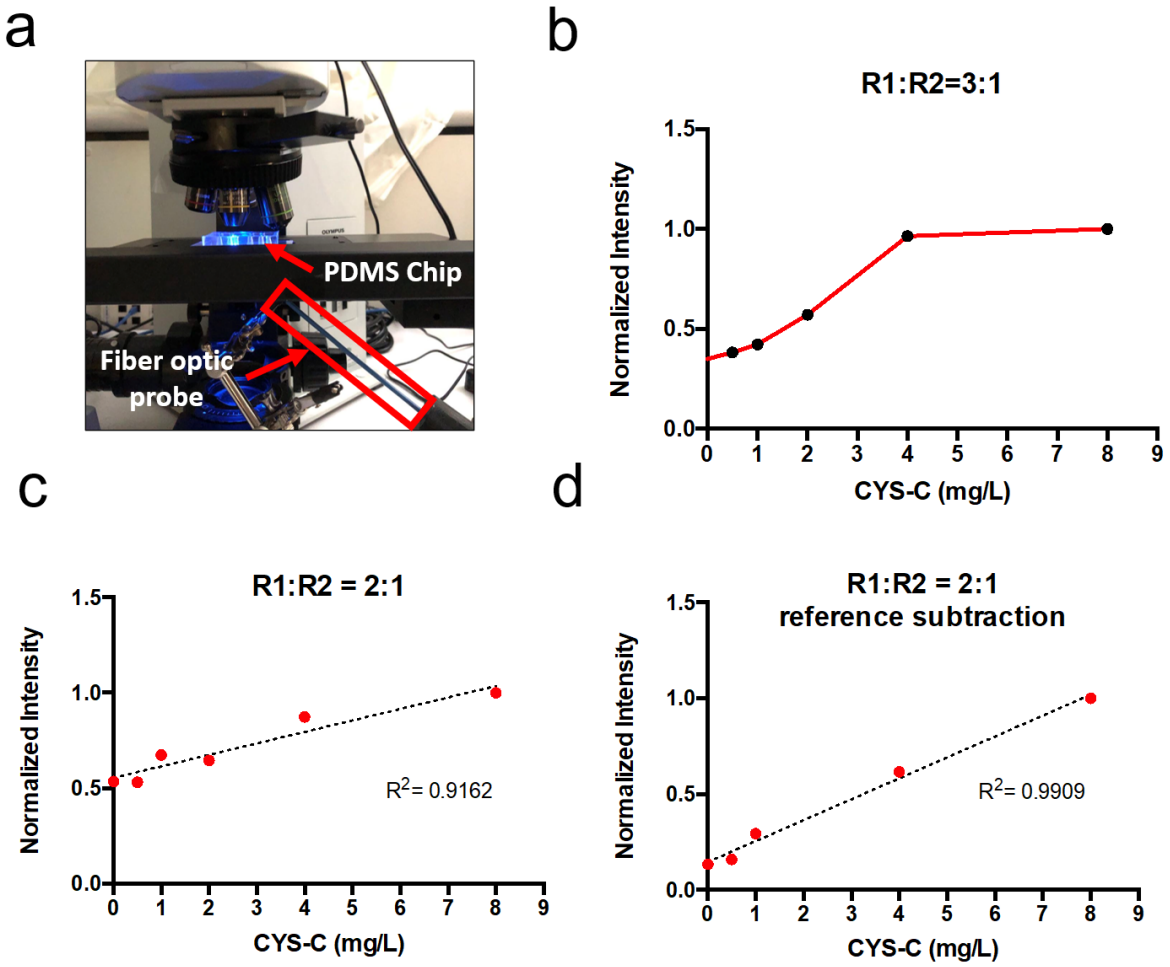

Figure 3.S1 CYS-C turbidity chip characterizations using the large microscope-based reader

a. Illustration of the microscope-based reader setup for side-scattered light measurements from the microfluidic chip; **b.** The calibration curve of the CYS-C turbidity chip test based on the 3:1 (R1:R2) reagent mixing ratio. R1 is the sample buffer; R2 is the CYS-C antibody-coated microparticle solution; **c.** Calibration curve of the CYS-C turbidity chip test based on the 2:1 (R1:R2) reagent mixing ratio; **d.** Calibration curve of the CYS-C turbidity chip test based on the 2:1 (R1:R2) reagent mixing ratio with the initial reference signal subtraction (i.e. the endpoint signal at the 13th minute minus the reference signal at the 3rd minute).

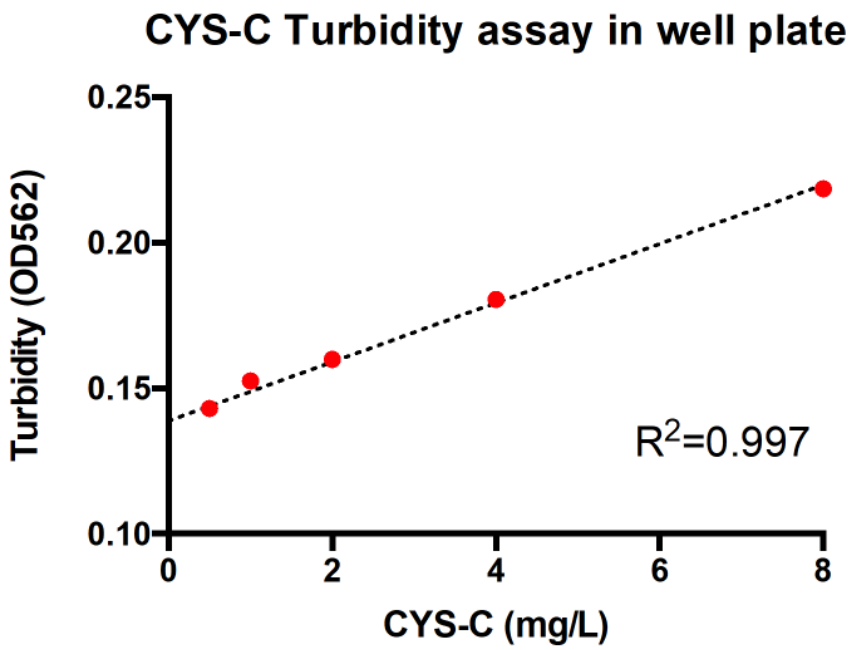

Figure 3.S2 The calibration curve of the CYS-C immunoturbidity assay using the 96-well plate and the plate reader as the reference test method.

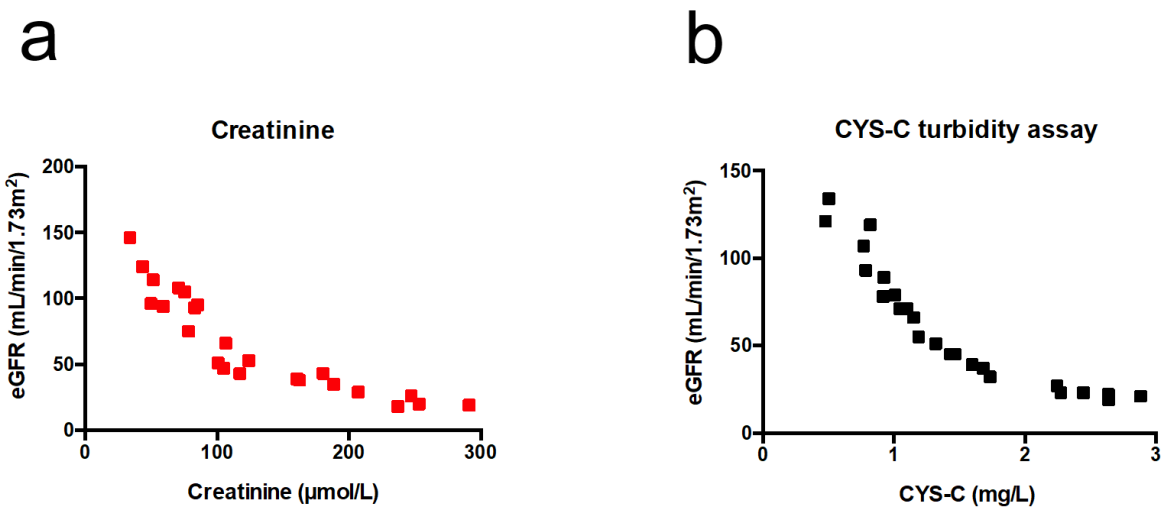

Figure 3.S3 Declining trend of eGFR against the respective serum filtration marker based on the filtration marker-specific estimation formula using the 24 clinical CKD samples.

A. eGFR vs clinically measured serum creatinine; **B.** eGFR vs turbidity chip measured serum CYS-C;

The cross-tabulation table for pairs of serum CYS-C eGFR level > 60, 30-59, <30ml/min/1.73m^2 and the reference standard of an eGFR from serum CRE

			clinical eGFR (serum CRE)		
			Positive	**Negative**	**Total**
CYS-C Turbidity chip tests	eGFR > 60	**Positive**	9	2	11
		Negative	2	11	13
		Total	11	13	24
	eGFR 30-59	**Positive**	4	3	7
		Negative	4	13	17
		Total	8	16	24
	eGFR <30	**Positive**	5	1	6
		Negative	1	17	18
		Total	6	18	24

Diagnostic accuracy of the turbidity chip results detections of eGFR > 60, 30-59, <30ml/min/1.73m^2 from serum CRE

		Sensitivity	**Specificity**	**PPV**	**NPV**	**Accuracy**
CYS-C Turbidity chip tests	eGFR > 60	82%	85%	82%	85%	83%
	eGFR is 30-59	50%	81%	57%	76%	71%
	eGFR < 30	83%	94%	83%	94%	92%

Table 3.S1 Three-stage (mild, moderate and severe) eGFR diagnosis accuracy based on the CYS-C chip test using the 24 clinical CKD samples.

Top. Cross-tabulation table comparing the CYS-C chip predicted eGFRcys-c against the clinical creatinine predicted eGFRcr is shown; **Bottom.** The accuracy evaluators based on data in the **Top** table including the sensitivity, specificity, PPV, NPV, and overall accuracy, are shown.

3.7 References

1. Inker, L. A., Schmid, C. H., Tighiouart, H., Eckfeldt, J. H., Feldman, H. I., Greene, T., Kusek, J. W., Manzi, J., Van Lente, F., Zhang, Y. L., Coresh, J., Levey, A. S. *"Estimating Glomerular Filtration Rate from Serum Creatinine and Cystatin C".* **New England Journal of Medicine** 2012, 367 (1), 20–29.

2. Lijo B. *"Creatinine Test vs Cystatin C Test".* **AGAPPE**. agappe.com/swiss_en/blog-details/creatinine-test-vs-cystatin-c-test.html.

3. Delgado, C., Baweja, M., Crews, D. C., Eneanya, N. D., Gadegbeku, C. A., Inker, L. A., Mendu, M. L., Miller, W. G., Moxey-Mims, M. M., Roberts, G. V., St. Peter, W. L. Warfield, C., Powe, N. R. *"A Unifying Approach for GFR Estimation: Recommendations of the NKF-ASN Task Force on Reassessing the Inclusion of Race in Diagnosing Kidney Disease".* **Journal of the American Society of Nephrology** 2021, 32 (12), 2994–3015.

4. Delgado, C., Baweja, M., Crews, D. C., Eneanya, N. D., Gadegbeku, C. A., Inker, L. A., Mendu, M. L., Miller, W. G., Moxey-Mims, M. M.; Roberts, G. V., St. Peter, W. L., Warfield, C., Powe, N. R. *"A Unifying Approach for GFR Estimation: Recommendations of the NKF-ASN Task Force on Reassessing the Inclusion of Race in Diagnosing Kidney Disease".* **American Journal of Kidney Diseases** 2022, 79 (2), 268-288.e1.

5. Inker, L. A., Eneanya, N. D., Coresh, J., Tighiouart, H., Wang, D., Sang, Y., Crews, D. C., Doria, A., Estrella, M. M., Froissart, M., Grams, M. E., Greene, T., Grubb, A.,

Gudnason, V., Gutiérrez, O. M., Kalil, R., Karger, A. B., Mauer, M., Navis, G., Nelson, R. G., Poggio, E. D., Rodby, R., Rossing, P., Rule, A. D., Selvin, E., Seegmiller, J. C., Shlipak, M. G., Torres, V. E., Yang, W., Ballew, S. H., Couture, S. J., Powe, N. R., Levey, A. S. *"New Creatinine- and Cystatin C–Based Equations to Estimate GFR without Race".* **New England Journal of Medicine** 2021, 385 (19), 1737–1749.

6. Kramer, H. J., Jaar, B. G., Choi, M. J., Palevsky, P. M., Vassalotti, J. A., Rocco, M. V. *"An Endorsement of the Removal of Race From GFR Estimation Equations: A Position Statement From the National Kidney Foundation Kidney Disease Outcomes Quality Initiative".* **American Journal of Kidney Diseases** 2022, 80 (6), 691–696.

7. Helmersson-Karlqvist, J., Lipcsey, M., Ärnlöv, J., Bell, M., Ravn, B., Dardashti, A., Larsson, A. *"Cystatin C Predicts Long Term Mortality Better than Creatinine in a Nationwide Study of Intensive Care Patients".* **Sci Rep** 2021, 11 (1), 5882.

8. Kaur, G., Levy, E. *"Cystatin C in Alzheimer's Disease".* **Front Mol Neurosci** 2012, *5*.

9. Mathews, P. M., Levy, E. *"Cystatin C in Aging and in Alzheimer's Disease".* **Ageing Res Rev** 2016, 32, 38–50.

10. van der Laan, S. W., Fall, T., Soumaré, A., Teumer, A., Sedaghat, S., Baumert, J., Zabaneh, D., van Setten, J., Isgum, I., Galesloot, T. E., Arpegård, J., Amouyel, P., Trompet, S., Waldenberger, M., Dörr, M., Magnusson, P. K., Giedraitis, V., Larsson, A., Morris, A. P., Felix, J. F., Morrison, A. C., Franceschini, N., Bis, J. C., Kavousi, M., O'Donnell, C., Drenos, F., Tragante, V., Munroe, P. B., Malik, R., Dichgans, M.,

Worrall, B. B., Erdmann, J., Nelson, C. P., Samani, N. J., Schunkert, H., Marchini, J., Patel, R. S., Hingorani, A. D., Lind, L., Pedersen, N. L., de Graaf, J., Kiemeney, L. A. L. M., Baumeister, S. E., Franco, O. H., Hofman, A., Uitterlinden, A. G., Koenig, W., Meisinger, C., Peters, A., Thorand, B., Jukema, J. W., Eriksen, B. O., Toft, I., Wilsgaard, T., Onland-Moret, N. C., van der Schouw, Y. T., Debette, S., Kumari, M., Svensson, P., van der Harst, P., Kivimaki, M., Keating, B. J., Sattar, N., Dehghan, A., Reiner, A. P., Ingelsson, E., den Ruijter, H. M., de Bakker, P. I. W., Pasterkamp, G., Ärnlöv, J., Holmes, M. V., Asselbergs, F. W. *"Cystatin C and Cardiovascular Disease".* **J Am Coll Cardiol** 2016, 68 (9), 934–945.

11. Xu, Y., Ding, Y., Li, X., Wu, X. *"Cystatin C Is a Disease-Associated Protein Subject to Multiple Regulation".* **Immunol Cell Biol** 2015, 93 (5), 442–451.

12. Zi, M., Xu, Y. *"Involvement of Cystatin C in Immunity and Apoptosis"*. **Immunol Lett** 2018, 196, 80–90.

13. Bikkarolla, S. K., Venkatesan, K., Revathy, Y. R., Parameswaran, S., Krishnakumar, S., Dendukuri, D. *"The Quantitative Detection of Cystatin-C in Patient Samples Using a Colorimetric Lateral Flow Immunoassay".* **Biosensors (Basel)** 2024, 14 (1), 30.

14. Tao, J., Zhao, P., Zeng, Q. *"The Determination of Cystatin C in Serum Based on Label-Free and near-Infrared Light Emitted PbS@BSA QDs".* **J Mater Chem B** 2016, 4 (24), 4258–4262.

15. Ujvari, S., Schwarzwald, C. C., Fouché, N., Howard, J., Schoster, A. *"Validation of a Point-of-Care Quantitative Equine IgG Turbidimetric Immunoassay and*

Comparison of IgG Concentrations Measured with Radial Immunodiffusion and a Point-of-Care IgG ELISA". **J Vet Intern Med** 2017, 31 (4), 1170–1177.

16. Gervais, L., de Rooij, N., Delamarche, E. "*Microfluidic Chips for Point-of-Care Immunodiagnostics".* **Advanced Materials** 2011, 23 (24).

17. Li, F., You, M., Li, S., Hu, J., Liu, C., Gong, Y., Yang, H., Xu, F. "Paper-Based Point-of-Care Immun*oassays: Recent Advances and Emerging Trends".* **Biotechnol Adv** 2020, 39, 107442.

18. Park, S., Zhang, Y., Lin, S., Wang, T.-H., Yang, S. *"Advances in Microfluidic PCR for Point-of-Care Infectious Disease Diagnostics".* **Biotechnol Adv** 2011, 29 (6), 830–839.

19. Chakraborty, T., Das, M., Lin, C. Y., Kao, C. H. *"Electrochemical Detection of Cystatin C by Oriented Antibody Immobilization on Streptococcal Protein G–Modified ZIF-8-Cu1−xNix(OH)2@Cu Core-Shell Nanostructured Electrode".* **Mater Today Chem** 2023, 27, 101273.

20. Trindade, E. K. G., Silva, B. V. M., Dutra, R. F. *"A Probeless and Label-Free Electrochemical Immunosensor for Cystatin C Detection Based on Ferrocene Functionalized-Graphene Platform".* **Biosens Bioelectron** 2019, 138, 111311.

21. Xia, M., Yang, P., Zhu, C., Hu, Y., Fang, L., Zheng, J., Wang, X., Li, Y. *"Highly Efficient Photoelectrochemical Detection of Cystatin C Based on a Core–Shell MOF Nanocomposite with Biomimetic-Catalysis Amplification".* **ACS Omega** 2024, 9 (26), 28228–28236.

22. Coliaie, P., Prajapati, A., Ali, R., Korde, A., Kelkar, M. S., Nere, N. K., Singh, M. R. *"Machine Learning-Driven, Sensor-Integrated Microfluidic Device for Monitoring and Control of Supersaturation for Automated Screening of Crystalline Materials".* **ACS Sens** 2022, 7 (3), 797–805.

23. Lucas, L. J., Han, J.-H., Chesler, J., Yoon, J.-Y. *"Latex Immunoagglutination Assay for a Vasculitis Marker in a Microfluidic Device Using Static Light Scattering Detection".* **Biosens Bioelectron** 2007, *22* (9–10), 2216–2222.

24. Huang, J., Zu, Y., Zhang, L., Cui, W. *"Progress in Procalcitonin Detection Based on Immunoassay".* **Research** 2024, 7.

25. Nilsen, T., Sunde, K., Larsson, A. *"A New Turbidimetric Immunoassay for Serum Calprotectin for Fully Automatized Clinical Analysers".* **J Inflamm** 2015, 12 (1), 45.

26. Slaets, J. I. F., Schmitter, P., Hilger, T., Lamers, M., Piepho, H.-P., Vien, T. D., Cadisch, G. *"A Turbidity-Based Method to Continuously Monitor Sediment, Carbon and Nitrogen Flows in Mountainous Watersheds".* **J Hydrol (Amst)** 2014, 513, 45–57.

27. Tomsa, D., Liu, Y., Stefanson, A., Ren, X., Sokoro, A. A. H., Komenda, P., Tangri, N., Zahedi, R. P., Rigatto, C., Lin, F. *"A Passive Flow Microreactor for Urine Creatinine Test".* **Microsyst Nanoeng** 2025, 11 (1), 56.

28. Orabona, E., Caliò, A., Rendina, I., Stefano, L., Medugno, M. *"Photomasks Fabrication Based on Optical Reduction for Microfluidic Applications".* **Micromachines (Basel)** 2013, 4 (2), 206–214.

29. Marmer, D. J., Hurtubise, P. E. "*17 - NEPHELOMETRIC AND TURBIDIMETRIC IMMUNOASSAY".* In *Immunoassay*; Diamandis, E. P., Christopoulos, T. K., Eds.; **Academic Press: San Diego,** 1996; pp 363–387.

30. Bland, J. M., Altman, D. G. *"Measuring Agreement in Method Comparison Studies".* **Stat Methods Med Res** 1999, 8 (2), 135–160.

31. Benoit, S. W., Ciccia, E. A., Devarajan, P. "*Cystatin C as a Biomarker of Chronic Kidney Disease: Latest Developments".* **Expert Rev Mol Diagn** 2020, 20 (10), 1019–1026.

32. Bargnoux, A.-S., Piéroni, L., Cristol, J.-P., Kuster, N., Delanaye, P., Carlier, M.-C., Fellahi, S., Boutten, A., Lombard, C., González-Antuña, A., Delatour, V., Cavalier, E. *"Multicenter Evaluation of Cystatin C Measurement after Assay Standardization"*. **Clin Chem** 2017, 63 (4), 833–841.

33. Eckfeldt, J. H., Karger, A. B., Miller, W. G., Rynders, G. P., Inker, L. A. *"Performance in Measurement of Serum Cystatin C by Laboratories Participating in the College of American Pathologists 2014 CYS Survey".* **Arch Pathol Lab Med** 2015, 139 (7), 888–893.

34. Seegmiller, J. C., Bachmann, L. M. *"Urine Albumin Measurements in Clinical Diagnostics".* **Clin Chem** 2024, 70 (2), 382–391.

35. Ma, Y.-C., Zuo, L., Chen, J.-H., Luo, Q., Yu, X.-Q., Li, Y., Xu, J.-S., Huang, S.-M., Wang, L.-N., Huang, W., Wang, M., Xu, G.-B., Wang, H.-Y. *"Improved GFR Estimation by Combined Creatinine and Cystatin C Measurements".* **Kidney Int** 2007, 72 (12), 1535–1542.

36. White, C., Akbari, A., Hussain, N., Dinh, L., Filler, G., Lepage, N.; Knoll, G. A. *"Estimating Glomerular Filtration Rate in Kidney Transplantation".* **Journal of the American Society of Nephrology** 2005, 16 (12), 3763–3770.

37. Sato, H., Kuroda, T., Tanabe, N., Ajiro, J., Wada, Y., Murakami, S., Sakatsume, M., Nakano, M., Gejyo, F. *"Cystatin C Is a Sensitive Marker for Detecting a Reduced Glomerular Filtration Rate When Assessing Chronic Kidney Disease in Patients with Rheumatoid Arthritis and Secondary Amyloidosis".* **Scand J Rheumatol** 2010, 39 (1), 33–37.

38. Pöge, U., Gerhardt, T., Stoffel-Wagner, B., Klehr, H. U., Sauerbruch, T., Woitas, R. P. *"Calculation of Glomerular Filtration Rate Based on Cystatin C in Cirrhotic Patients".* **Nephrology Dialysis Transplantation** 2006, 21 (3), 660–664.

39. Bouvet, Y., Bouissou, F., Coulais, Y., Séronie-Vivien, S., Tafani, M., Decramer, S., Chatelut, E. *"GFR Is Better Estimated by Considering Both Serum Cystatin C and Creatinine Levels".* **Pediatric Nephrology** 2006, 21 (9), 1299–1306.

40. Stevens, L. A., Coresh, J., Schmid, C. H., Feldman, H. I., Froissart, M., Kusek, J., Rossert, J., Van Lente, F., Bruce, R. D., Zhang, Y. (Lucy), Greene, T., Levey, A. S. *"Estimating GFR Using Serum Cystatin C Alone and in Combination With Serum Creatinine: A Pooled Analysis of 3,418 Individuals With CKD".* **American Journal of Kidney Diseases** 2008, 51 (3), 395–406.

41. Chen, D. C., Potok, O. A., Rifkin, D., Estrella, M. M. *"Advantages, Limitations, and Clinical Considerations in Using Cystatin C to Estimate GFR".* **Kidney360** 2022, 3 (10), 1807–1814.

42. Karger, A. B., Long, T., Inker, L. A., Eckfeldt, J. H. *"Improved Performance in Measurement of Serum Cystatin C by Laboratories Participating in the College of American Pathologists 2019 CYS Survey"*. **Arch Pathol Lab Med** 2022, 146 (10), 1218–1223.

43. Giavarina, D. *"Understanding Bland Altman Analysis"*. **Biochem Med (Zagreb)** 2015, *25* (2), 141–151.

44. Grubb, A., Blirup-Jensen, S., Lindström, V., Schmidt, C., Althaus, H., Zegers, I. *"First Certified Reference Material for Cystatin C in Human Serum ERM-DA471/IFCC"*. **Clin Chem Lab Med** 2010, 48 (11), 1619–1621.

45. Peralta, C. *A. "Detection of Chronic Kidney Disease With Creatinine, Cystatin C, and Urine Albumin-to-Creatinine Ratio and Association With Progression to End-Stage Renal Disease and Mortality"*. **JAMA** 2011, 305 (15), 1545.

46. Stevens, L. A., Padala, S., Levey, A. S. *"Advances in Glomerular Filtration Rate-Estimating Equations"*. **Curr Opin Nephrol Hypertens** 2010, 19 (3), 298–307.

47. Shaikh, S. A. *"Measures Derived from a 2 x 2 Table for an Accuracy of a Diagnostic Test"*. **J Biom Biostat** 2011, 02 (05).

Chapter 4: Conclusion

The growing number of CKD patients around the globe is an indicator that the current diagnostic tools require an update to make them as accessible as possible for detecting the earliest signs of CKD. Though it is common knowledge that early diagnostics of any disease can have a fundamental and positive impact on patients' quality of life, the application of techniques, instruments, methods, and principles described in this work is not and should not be limited to creatinine, albumin, or CYS-C only. The large variety of diseases that are affecting people on every continent, country, and social group demands innovative diagnostic approaches that are both accurate and accessible.

The microfluidic platform developed in this research, particularly the uCR-Chip for creatinine detection and the CYS-C chip for turbidimetric measurements, demonstrates the potential of miniaturized systems for PoC diagnostics. These platforms offer numerous advantages, including reduced sample volumes, fast analysis times, lower reagent consumption, and enhanced portability–all critical factors for widespread implementation in resource-limited settings.

Looking forward, the versatility of these microfluidic systems presents exciting opportunities for expansion beyond CKD biomarkers. The foundational technologies developed here could be readily adapted for detecting cardiovascular disease markers, liver function indicators, cancer biomarkers, and infectious disease agents. Furthermore, integration with digital health platforms and telemedicine systems could create comprehensive diagnostic ecosystems that connect remote testing with specialist care, regardless of geographical barriers.

Future work should focus on multiplexing capabilities to simultaneously measure multiple biomarkers from a single sample, enhancing the diagnostic power and efficiency of this technology. The further development of uCR-Chip should combine it with uAL-Chip (urinary albumin chip) and the CYS-C chip in one CKD-Chip for a more comprehensive one-step test. As the assays often use different methods of detection (colorimetric, fluorometric, turbidimetric), the development of a miniature reader capable of performing more than 1 type of signal will significantly advance point-of-care CKD diagnostics by enabling comprehensive biomarker analysis without the need for multiple specialized instruments. Additionally, exploring sustainable manufacturing methods and materials would further reduce costs and environmental impact, making these tools truly accessible to global populations. As microfluidic diagnostic platforms continue to mature, they hold promise not just for transforming CKD management but for fundamentally reshaping how we approach early disease detection across the medical spectrum.